Inorg. Chem. **2008**, *47*, 8242−8257

Inorganic Chemistry
Article

Photophysical Properties of Platinum(II)−Acetylide Complexes: the Effect of a Strongly Electron-Accepting Diimine Ligand on Excited-State Structure

Christopher J. Adams,*,† Natalie Fey,† Zoë A. Harrison,† Igor V. Sazanovich,‡ Michael Towrie,§ and Julia A. Weinstein*,‡

School of Chemistry, University of Bristol, BRISTOL BS8 1TS, U.K., Department of Chemistry, University of Sheffield, SHEFFIELD S3 7HF, U.K., and Central Laser Facility, Science and Technology Facilities Council, Rutherford Appleton Laboratory, Chilton, Didcot, Oxfordshire OX11 0QX, U.K.

Received May 9, 2008

The compounds [Pt(MesBIAN)(−C≡C−R)$_2$] (R = C_6H_4−CN-*p*, **1**; $SiMe_3$, **2**; C_6H_4−CF_3-*p*, **3**; C_6H_5, **4**; C_6H_4−CH_3-*p* **5**) {MesBIAN = bis(mesitylimino)acenaphthene} have been synthesized; the X-ray crystal structure determinations of **4** and **5** and the starting material [Pt(MesBIAN)Cl_2] are reported. Chemical oxidation of **4** with diiodine leads to generation of an intermediate platinum(IV) bis(acetylide) diiodide complex, which then couples and reductively eliminates the acetylide ligands as a diyne, leading to the generation of [Pt(MesBIAN)I_2] **6**. Compound **2** readily forms an adduct **2a** with copper(I) chloride, in which the copper atom is bonded to the two acetylide triple bonds. **1**−**5** each undergo an irreversible oxidation, and a reversible one-electron reduction to generate a stable anion. ESR studies of **1**$^-$−**5**$^-$ show that the unpaired electron is localized mainly on the π^* orbital of the coordinated MesBIAN ligand, with about 10% platinum contribution to the singly occupied molecular orbital (SOMO). The compounds show a strong absorption at around 500 nm in the UV/visible spectrum, which is assigned to a "mixed metal−ligand to ligand charge transfer" (MMLL′CT) transition; this assignment is supported by time-dependent density-functional theory (TD-DFT) calculations on **5**. **1**−**5** emit in the near-infrared region from a ^{3}MMLL′CT excited state, with lifetimes ranging from 8 to 36 ns. Picosecond and nanosecond time-resolved infrared (TRIR) spectroscopy has been used to probe directly the nature and dynamics of the excited state of **5.** The TRIR data show a decrease of the energy of the C≡C vibration upon excitation, by about 90 cm^{-1} in comparison to the ground state, and formation of a new, very intense, and very broad band at 1820 cm^{-1}. We propose that the excited-state structure contains some contribution from a pseudo-cumulenic form of the platinum-acetylide moiety, which is supported by TD-DFT calculations. Picosecond TRIR allowed determination of the rate of vibrational relaxation (14 ps) of the vibrationally "hot" electronic excited state of **5** formed upon initial laser excitation.

Introduction

Square-planar platinum(II) complexes are now playing an increasingly important role in the development of transition metal complexes for photoapplications, a research area which is presently dominated by chromophores with octahedral d^6 metal centers. Since the first report of a platinum-diimine compound with acetylide co-ligands,[1] interest in the field has exploded and photoapplications of such compounds now include energy transfer, sensitization of lanthanide-based emission in multinuclear assemblies,[2,3] triggering of photocyclization,[4] generation of charge-separated excited states in systems for artificial photosynthesis,[5] and many others. These developments have been driven by the attractive

* To whom correspondence should be addressed. E-mail: chcja@bris.ac.uk.
† University of Bristol.
‡ University of Sheffield.
§ Rutherford Appleton Laboratory.

(1) Chan, C. W.; Cheng, L. K.; Che, C. M. *Coord. Chem. Rev.* **1994**, *132*, 87–97.
(2) Kennedy, F.; Shavaleev, N. M.; Koullourou, T.; Bell, Z. R.; Jeffery, J. C.; Faulkner, S.; Ward, M. D. *Dalton Trans.* **2007**, 1492–1499.
(3) Shavaleev, N. M.; Accorsi, G.; Virgili, D.; Bell, D. R.; Lazarides, T.; Calogero, G.; Armaroli, N.; Ward, M. D. *Inorg. Chem.* **2005**, *44*, 61–72.

10.1021/ic800850h CCC: $40.75
Published on Web 08/09/2008

photophysical features of these complexes, which include absorption of a significant part of the visible spectrum, relatively long-lived excited states, and good photochemical stability. Coordinatively unsaturated platinum(II) complexes may also partake in photochemical reactions through the vacant axial coordination sites on the metal, which is not possible for systems based on octahedral d^6-metal chromophores.

Many of the above applications are based on the long-lived room temperature luminescence exhibited by these compounds—a property which may be readily tuned by modifying the diimine ligand and by changing the functional groups on the acetylide. In the majority of cases, the highest occupied molecular orbital (HOMO) in such compounds is based upon a combination of acetylide π and metal d orbitals, whereas the lowest unoccupied molecular orbital (LUMO) is based largely upon a diimine π^* orbital. The electronic transition between the two may be termed a "mixed metal−ligand to ligand charge transfer" (MMLL′CT) transition. The initial formation of a ^{1}MMLL′CT state upon photoexcitation is followed by rapid singlet to triplet intersystem crossing because of the presence of the heavy metal atom, generating a long-lived ^{3}MMLL′CT excited state, decay of which is responsible for the observed luminescence. Thus, the energy and lifetime of the emission may be varied as the energy of the HOMO can be altered by substitution of the terminal groups on the acetylide ligand, and the energy of the LUMO by modification of the diimine.[6]

The luminescence and electronic absorption properties of platinum(II)−acetylide systems have been studied extensively, but electronic spectroscopy alone does not necessarily yield information on the structures of the excited states that largely determine such properties. Vibrational spectroscopy, in particular time-resolved infrared (TRIR) spectroscopy, provides a complementary means to directly probe excited-state structure. To date, TRIR spectroscopy only appears to have been applied to two platinum(II)−acetylide systems.[7−9]

Within this context, we have recently reported preliminary studies on the first platinum(II)−diimine−acetylide compounds containing a strongly accepting diimine ligand with exocyclic *N*-donor atoms, namely, bis(mesitylimino)acenaphthene (abbreviated MesBIAN). By comparison with *N*-heterocyclic ligands such as bipyridine, MesBIAN has a much lower energy π^* LUMO, giving its platinum compounds a comparatively small HOMO−LUMO gap. The immediate obvious effect of this is a shift of the emission energy of the triplet excited state from the visible into the near-infrared region of the spectrum, which is potentially important for imaging of biological objects. A second effect is to allow emission from the charge-transfer states of complexes with low-field ligands such as chloride: the low energy LUMO localized on the MesBIAN ligand ensures that the emissive charge-transfer state is the lowest in energy and is not quenched by a nonemissive d−d state. The nature of the MesBIAN ligand further facilitates the emission because of its relative rigidity and the steric protection it affords the axial sites of the metal, preventing radiationless deactivation through solvent interaction.

Our preliminary communication reported luminescence from compounds [Pt(MesBIAN)(LL)], where LL = Cl_2, 1,2-dithiooxalate, and (−C≡C−C_6H_4−CF_3-*p*)$_2$.[10] We have recently reported our studies on a series of 1,2-dithiolate complexes[11] and below we consider a range of platinum(II)−MesBIAN−acetylide compounds, whose lowest triplet charge-transfer excited state emits in the NIR range while retaining a long enough lifetime for bimolecular reactions to occur. We investigate the structure of the excited state by TRIR spectroscopy and correlate the experimental findings with the results of time-dependent density-functional theory (TD-DFT) calculations, which predict structural changes in the triplet excited state of the platinum(II)−acetylides in question.

Results and Discussion

Syntheses and Characterization. The platinum(II)−MesBIAN−acetylide compounds [Pt(MesBIAN)(−C≡C−R)$_2$] (R = C_6H_4−CN-*p*, **1**; $SiMe_3$, **2**; C_6H_4−CF_3-*p*, **3**; C_6H_5, **4**; C_6H_4−CH_3-*p*, **5**) were readily synthesized by the copper(I) catalyzed reaction of [Pt(MesBIAN)Cl_2] with the appropriate terminal alkyne (Scheme 1). The compounds were generally isolated in good yield following purification by column chromatography and crystallization and were characterized by elemental analysis, mass spectrometry, and ^{1}H NMR and IR spectroscopies (Table 1). The yield of **2** was somewhat lower than for the remaining compounds. This appears to be due to the facile formation of an adduct with the copper(I) ions present in the solution, in which the copper(I) ion is coordinated between the acetylide triple bonds in a pincer fashion,[12,13] with a chloride ion originating from the platinum starting material completing the copper coordination sphere. This compound, [{Pt(MesBIAN)(−C≡C−$SiMe_3$)$_2$}-η^2,η^2-CuCl] **2a**, was also independently and deliberately synthesized and fully characterized. The C≡C stretching frequencies of **2a** are reduced by some 65 cm^{-1} compared to **2** (Table 1), consistent with donation of electron density from the triple bond to the copper atom. There is also a marked change in the shift of the trimethylsilyl group in the ^{1}H NMR spectrum from −0.17 to −0.01 p.p.m., whereas the other signals remain largely unchanged (Table 1).

The X-ray crystal structure of **4**, containing two $CDCl_3$ solvent molecules, has been determined (Figure 1), and

(4) Lee, J. K. W.; Ko, C. C.; Wong, K. M. C.; Zhu, N. Y.; Yam, V. W. W. *Organometallics* **2007**, *26*, 12–15.
(5) Chakraborty, S.; Wadas, T. J.; Hester, H.; Schmehl, R.; Eisenberg, R. *Inorg. Chem.* **2005**, *44*, 6865–6878.
(6) Hissler, M.; Connick, W. B.; Geiger, D. K.; McGarrah, J. E.; Lipa, D.; Lachicotte, R. J.; Eisenberg, R. *Inorg. Chem.* **2000**, *39*, 447–457.
(7) Cooper, T. M.; Blaudeau, J. P.; Hall, B. C.; Rogers, J. E.; McLean, D. G.; Liu, Y. L.; Toscano, J. P. *Chem. Phys. Lett.* **2004**, *400*, 239–244.
(8) Whittle, C. E.; Weinstein, J. A.; George, M. W.; Schanze, K. S. *Inorg. Chem.* **2001**, *40*, 4053–4062.
(9) Emmert, L. A.; Choi, W.; Marshall, J. A.; Yang, J.; Meyer, L. A.; Brozik, J. A. *J. Phys. Chem. A* **2003**, *107*, 11340–11346.
(10) Adams, C. J.; Fey, N.; Weinstein, J. A. *Inorg. Chem.* **2006**, *45*, 6105–6107.
(11) Adams, C. J.; Fey, N.; Parfitt, M.; Pope, S. J. A.; Weinstein, J. A. *Dalton Trans.* **2007**, 4446–4456.
(12) Adams, C. J.; Raithby, P. R. *J. Organomet. Chem.* **1999**, *578*, 178–185.
(13) Yamazaki, S.; Deeming, A. J. *J. Chem. Soc., Dalton Trans.* **1993**, 3051–3057.

Scheme 1. Synthesis and Structures of **1**−**5**

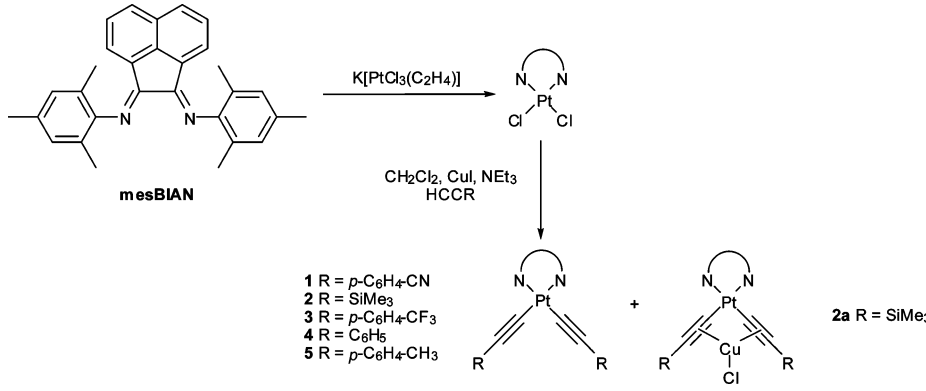

Table 1. ^{1}H NMR, IR, and Analytical Data for All Compounds

	compound	^{1}H NMR data[a]	ν(CC)[b]/cm^{-1}	microanalytical data
1	Pt(Mes-BIAN)(-CC-$C_6H_4CN)_2$	δ = 2.36 (12H, s, Me); 2.43 (6H, s, Me); 6.88 (4H, d, J = 8.5 Hz); 6.99 (2H, d, J = 7.2 Hz); 7.11 (4H, s); 7.36 (4H, d, J = 8.2 Hz); 7.54 (2H, t, J = 7.3 Hz); 8.24 (2H, d, J = 8.2 Hz)	2126sh, 2116 [ν(CN) = 2225]	Calcd: C, 66.73; H, 4.20; N, 6.49%. Found: C, 66.79; H, 3.82; N, 6.26%.
2	Pt(Mes-BIAN)(-CC-$SiMe_3)_2$	δ = −0.17 (18H, s); 2.29 (12H, s, Me); 2.42 (6H, s, Me); 6.90 (4H, d, J = 7.35 Hz); 7.04 (4H, s); 7.46 (2H, t, J = 8.3 Hz); 8.17 (2H, d, J = 8.2 Hz)	2057, 2043	Calcd: C, 59.60; H, 5.75; N, 3.48%. Found: C, 59.44; H, 5.90; N, 3.08%.
2a	{Pt(Mes-BIAN)(-CC-$SiMe_3)_2CuCl\}_2$	δ = −0.01 (18H, s); 2.33 (12H, s, Me); 2.42 (6H, s, Me); 6.94 (4H, d, J = 7.1 Hz); 7.09 (4H, s); 7.52 (2H, t, J = 7.5 Hz); 8.21 (2H, d, J = 8.4 Hz)	1990, 1979	Calcd: C,53.08; H, 5.12; N, 3.10%. Found: C, 53.29; H, 5.20; N, 3.67%.
3	Pt(Mes-BIAN)(-CC-$C_6H_4CF_3)_2$	δ = 2.37 (12H, s, Me); 2.43 (6H, s, Me); 6.92 (4H, d, J = 8.1 Hz); 6.98 (2H, d, J = 7.1 Hz); 7.11 (4H, s); 7.32 (4H, d, J = 8.4 Hz); 7.52 (2H, t, J = 8.1 Hz); 8.22 (2H, d, J = 8.4 Hz)	2126sh, 2118	Calcd: C, 60.69; H, 3.82; N, 2.95%. Found: C, 60.59; H, 3.68; N, 2.65%.
4	Pt(Mes-BIAN)(-CC-$C_6H_5)_2$	δ = 2.37 (12H, s, Me); 2.44 (6H, s, Me); 6.87 (4H, d, J = 7.3 Hz); 6.98 (4H, m); 7.08 (8H, m); 7.49 (2H, t, J = 7.9 Hz); 8.21 (2H, d, J = 8.1 Hz)	2127sh, 2116	Calcd: C, 67.88; H, 4.71; N, 3.44%. Found: C, 67.75; H, 4.62; N, 3.13%.
5	Pt(Mes-BIAN)(-CC-$C_6H_4CH_3)_2$	δ = 2.27 (6H, s, Me); 2.36 (12H, s, Me); 2.45 (6H, s, Me); 6.75 (4H, d, J = 8.3 Hz); 6.88 (4H, d, J = 8.1 Hz); 6.95 (2H, d, J = 7.4 Hz); 7.10 (4H, s); 7.47 (2H, t, J = 7.3 Hz); 8.20 (2H, d, J = 8.3 Hz)	2124sh, 2115	Calcd: C, 68.47; H, 5.03; N, 3.33%. Found: C, 68.21; H, 5.07; N, 3.05%.
6	Pt(Mes-BIAN)I_2	δ = 2.31 (12H, s, Me); 2.46 (6H, s, Me); 6.78 (2H, d, J = 7.3 Hz); 7.12 (4H, s); 7.46 (2H, t, J = 7.8 Hz); 8.28 (2H, d, J = 8.3 Hz)	-	Calcd: C, 41.63; H, 3.26; N, 3.24%. Found: C, 41.64; H, 3.33; N, 2.82%.

[a] Recorded at 300 MHz in $CDCl_3$, and reported in ppm vs. $SiMe_4$. [b] Recorded in CH_2Cl_2 solution.

selected bond lengths and angles are presented in Table 2. The platinum atom has an approximately square-planar geometry, with the major deviation being due to the small bite angle of the MesBIAN chelate (79°). The mesityl rings of the MesBIAN ligand are perpendicular to the biazanaphthene unit. The two phenylacetylide ligands are not quite linear, bowing slightly away from each other {Pt(1)−C(31)−C(32) = 174.4(9)°; Pt(1)−C(39)−C(40) = 172.1(9)°}, with the phenyl rings twisted out of the plane defined by the acenaphthene unit and the platinum atom by 68 and 75°. The most interesting feature is the location of the two solvate molecules of $CDCl_3$, which are positioned to allow their deuterium atoms to hydrogen bond to the two carbon−carbon triple bonds (Table 3). Each deuterium atom is hydrogen bonded to both acetylide triple bonds, being nearer to the carbon atom bound to the platinum atom, at a distance at or below the sum (2.9 Å) of the van der Waals radii of hydrogen and carbon. This interaction between chlorinated solvent molecules and triple bonds has been noted before and used as the basis for studies into vapoluminescent behavior.[14] The molecules of **4** are packed within the structure in a one-dimensional chain (Figure 2), and these chains are themselves

(14) Lu, W.; Chan, M. C. W.; Zhu, N. Y.; Che, C. M.; He, Z.; Wong, K. Y. *Chem.*−*Eur. J.* **2003**, *9*, 6155–6166.

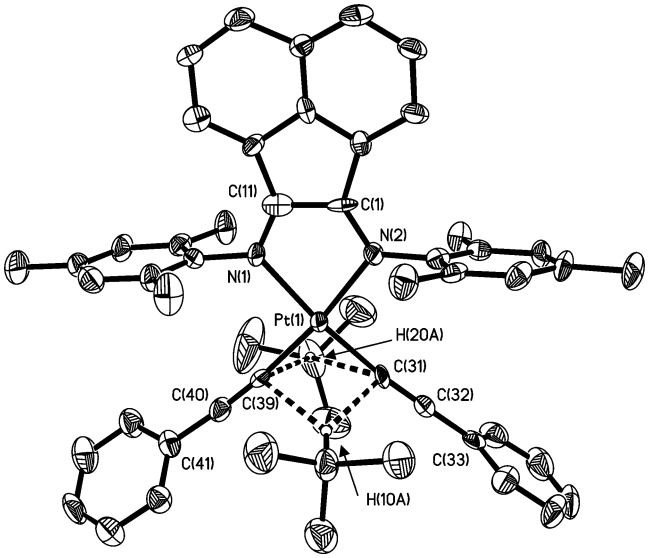

Figure 1. Structure of **4**·2$CDCl_3$, showing how the two $CDCl_3$ solvent molecules hydrogen-bond to the acetylide triple bonds. Ellipsoids at the 50% probability level.

Table 2. Selected Bond Lengths (Å) and Angles (deg) for Crystallographically Determined Structures

	4·2$CHCl_3$	**5**	[Pt(MesBIAN)Cl_2]·Et_2O
Pt(1)−N(1)	2.098(2)	2.071(3)	2.019(3)
Pt(1)−N(2)	2.087(8)	2.073(3)	2.024(3)
Pt(1)−C(31)	1.941(10)	1.959(3)	
Pt(1)−C(39)	1.946(10)	1.944(3)	
C(31)−C(32)	1.216(14)	1.200(4)	
C(39)−C(40)	1.192(14)	1.202(4)	
C(32)−C(33)	1.443(14)	1.446(4)	
C(40)−C(41)	1.457(14)	1.441(4)	
C(1)−N(2)	1.304(12)	1.292(4)	1.285(3)
C(11)−N(1)	1.274(12)	1.295(4)	1.293(6)
C(1)−C(11)	1.458(15)	1.482(4)	1.489(6)
Pt(1)−C(31)−C(32)	174.4(9)	173.6(3)	
Pt(1)−C(39)−C(40)	172.1(9)	173.1(3)	
C(31)−C(32)−C(33)	178.2(13)	177.1(4)	
C(39)−C(40)−C(41)	176.2(11)	178.5(3)	
C(39)−Pt(1)−C(31)	92.0(4)	91.50 (12)	
N(1)−Pt(1)−N(2)	79.0(3)	79.37(9)	80.96(4)
Cl(1)−Pt(1)−Cl(2)			91.12(4)

Table 3. Hydrogen-Bond Distances between the Hydrogen Atoms of Chloroform Solvent Molecules and the Carbon Atoms of Acetylenic Triple Bonds in the Structure of **4**·2$CHCl_3$

	H(10A)	H(20A)
C(31)	2.52	2.91
C(32)	3.11	3.55
C(39)	2.74	2.51
C(40)	3.32	3.08

arranged in an approximately hexagonal arrangement. This then creates channels parallel to the chains, which are where the chloroform molecules lie (Figure 3).

The X-ray structures of **5** and of the starting material [Pt(MesBIAN)Cl_2] (as a diethylether solvate) have also been determined (Table 2; pictures are shown in the Supporting Information). The gross structure of **5** is very similar to that of **4**; equivalent bond lengths are within 0.03 Å, and angles within 2°. The major difference between [Pt(MesBIAN)Cl_2] and **4** and **5** is in the Pt−N distances, which are in the 2.07 to 2.10 Å range for the acetylide structures but which are only 2.02 Å for the dichloride, showing the strong *trans*-influence of the carbon-donor ligand.

Cyclic Voltammetry, ESR, and IR Electrochemical Studies. To elucidate the nature of the frontier orbitals of **1**−**5** (spectro)electrochemical studies were performed. Cyclic voltammetry reveals that the first oxidation process for **1**−**5** lies between 1.2 and 1.6 V versus SCE (Table 4) and is irreversible. The value of $E_{p,a}$ is strongly affected by the acetylide, indicating considerable involvement of acetylide-based orbitals in the oxidation process. This suggestion is consistent with the 32% of the acetylide π-system involvement in the HOMO obtained by density-functional theory (DFT) calculations for **5** (Table 7, vide infra). The value of 1.31 V for **4** is very similar to that of 1.36 V for [Pt(dbbpy)(−C≡C−Ph)$_2$] {dbbpy = 4,4′-*tert*-butyl-2,2′-bipyridine},[15] also indicating that the identity of the diimine ligand is relatively unimportant in determining the nature of the HOMO.

Each of the compounds **1**−**5** undergoes a fully reversible first reduction between −0.67 and −0.78 V and a second, irreversible process at −1.5 V or beyond. The values of the first reduction potential are similar for all the compounds studied and are very close to that of [Pt(MesBIAN)Cl_2] (−0.60 V vs SCE),[10] indicating the predominant MesBIAN localization of the reduction process. The value of −0.74 V for **4** compares to −1.36 V for [Pt(dbbpy)(−C≡C−Ph)$_2$],[15] showing that (in contrast to the HOMO) the energy of the LUMO is greatly affected by the diimine. The value of the first reduction potential becomes marginally more negative as the donor capability of the aromatic acetylides increases (**1** < **3** < **4** < **5**); the same trend is observed for the second reduction process.

Because the monoanions **1**$^-$−**5**$^-$ are stable, it is possible to probe further the composition of the LUMO by ESR spectroscopy. The ESR spectra of the anions **1**$^-$−**5**$^-$ were recorded on 2:1 THF/CH_2Cl_2 solutions of the compounds, chemically reduced with decamethylcobaltocene *in situ* in an ESR tube. In fluid solution all the ESR spectra consist of a single broad peak, with no discernible platinum satellites. In contrast, in frozen glass at 110 K a well defined rhombic spectrum is observed, with ^{195}Pt satellites on the two low field g components, and coupling to the two nitrogen atoms of the MesBIAN ligand on the high field component. Figure 4 shows the spectrum of **3**$^-$ as a representative example, and g and A values for all complexes are presented in Table 5. Assignment of these values follows the methodology of McInnes and co-workers, which also allows for calculation of the values of a^2 and b^2, the coefficients of the $5d_{yz}$ and $6p_z$ orbitals, respectively, in the singly occupied molecular orbital (SOMO).[16−18]

(15) Hua, F.; Kinayyigit, S.; Cable, J. R.; Castellano, F. N. *Inorg. Chem.* **2006**, *45*, 4304–4306.

(16) Throughout this paper, we use a coordinate system with the *y*-axis bisecting the diimine and dithiolate ligands (i.e., the C_2 rotational axis), the *z*-axis perpendicular to the plane of the molecule, and the *x* axis perpendicular to *y* and *z*.

(17) McInnes, E. J. L.; Farley, R. D.; Macgregor, S. A.; Taylor, K. J.; Yellowlees, L. J.; Rowlands, C. C. *J. Chem. Soc., Faraday Trans.* **1998**, *94*, 2985–2991.

Figure 2. One-dimensional chain formed by **4** in the solid state.

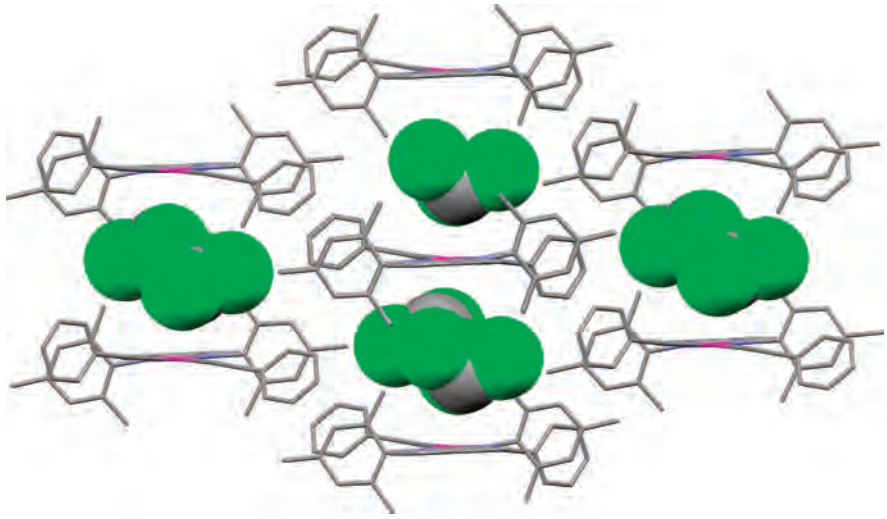

Figure 3. Chloroform solvate molecules (green and gray space-filling) occupy the channels created by the hexagonal arrangement of chains of **4** in the solid state.

Table 4. Optical and Electrochemical Data for **1**−**5**[a]

	λ_{max}^{abs}/nm (ε/10^4 M^{-1} cm^{-1})	λ_{max}^{em}/nm(Δ/cm^{-1})[b]	ϕ /10^{-3} [e]	τ/ns	k_r/10^5 s^{-1} [f]	k_{nr}/10^7 s^{-1} [g]	E_{red}^1/V	$E_{p,c}^2$/V	$E_{p,a}$/V	$E_{p,a} - E_{red}^1$/V
1	508 (1.39), 719 (0.025)	786 (1305), 873	5.3	36	1.47	2.76	−0.67	−1.52	1.60	2.27
2	477 (0.94), 514 (0.96), 723 (0.013)	790 (1342), 884	3.7	32	1.15	3.10	−0.78	−1.69	1.49	2.27
3	514 (1.11), 720 (0.027)	800 (1317), 893[c]	0.8	30	0.27	3.30	−0.69	−1.74	1.53	2.22
4	527 (1.11), 756 (0.027)	848, 937	0.2	10	0.20	9.99	−0.74	−1.73	1.31	2.05
5	535 (1.21), 561 (1.01), 773 (0.038)	896[d]	0.09	8	0.11	12.5	−0.77	−1.73	1.20	1.97

[a] Voltammetric potentials are referenced to SCE; the first reduction of each compound is reversible, whereas the second reduction and the oxidation are irreversible. [b] Obtained from multi-Gaussian deconvolution of the spectral profile. The numbers in brackets refer to the spacing of the two vibrational components. [c] We have previously reported an emission maximum of 800 nm for **3**.[10] An enhanced emission detector allowed us to investigate the NIR region, and therefore detect an 893 nm shoulder in the emission spectrum that was not previously detected. A small contribution from a 938 nm band is also resolved upon Gaussian deconvolution. [d] A small contribution from a 985 nm band is resolved upon Gaussian deconvolution. [e] ϕ determined using [Pt(MesBIAN)Cl_2] ($\phi = 3 \times 10^{-4}$ in deoxygenated CH_2Cl_2) and [Ru(bpy)$_3$]Cl_2 ($\phi = 0.028$ in aerated H_2O) as emission standards. [f] Radiative decay rate, calculated as $k_r = \phi_{em}/\tau_{em}$. [g] Nonradiative decay rate, calculated as $k_{nr} = (1 - \phi_{em})/\tau_{em}$.

Table 5. g-Values, Hyperfine Coupling Constants, and ν(CC) Stretching Frequencies for the Radical Anions **1**$^-$−**5**$^-$[a]

	g_{iso}	g_y	g_x	g_z	$\langle g \rangle$	A_y(Pt)	A_x(Pt)	A_z(Pt)	$\langle A \rangle$	A_z(N)	$100a^2$	$100b^2$	ν(CC)/cm^{-1}	$\Delta\nu$(CC)[c]/cm^{-1}
1$^-$	2.004	2.028	2.006	1.976	2.003	−47	−48	−5	−33.33	12.5	0.21	8.70	2107, 2090, 2048w [b]	−21,−26
2$^-$	2.005	2.033	2.006	1.975	2.005	−48	−50	−5	−34.33	12	0.42	8.91	2039, 2019	−18,−24
3$^-$	2.004	2.030	2.006	1.975	2.004	−46.75	−50	−6	−34.25	12.5	0.69	8.44	2110, 2096, 2044w	−16,−22
4$^-$	*d*	2.036	2.007	1.974	2.005	−47	−50	−5	−34	13	0.63	8.71	2110, 2097	−17,−19
5$^-$	2.006	2.038	2.005	1.975	2.006	−47	−50	−5	−34	13	0.63	8.71	2110, 2098, 2049w	−14,−17

[a] $100a^2$ and $100b^2$ are the percentage contributions to the SOMO of the platinum 5d and 6p orbitals, respectively. Hyperfine coupling constants are given in units of 10^{-4} cm^{-1}. [b] Also shows ν(CN) at 2222 cm^{-1}; $\Delta\nu$(CN) = −3 cm^{-1}. [c] Shift upon reduction of the neutral compounds. [d] At room temperature, the spectrum was not isotropic.

The hyperfine coupling constants of the anions indicate a contribution of 9 to 10% of metal orbitals to the SOMO (Table 5). This is in agreement with the DFT-calculated metal contribution of 7% to the LUMO in neutral **5** (below). One noteworthy feature of the spectra is the similarity of the coupling constants A_x and A_y to each other. The contribution of the $5d_{yz}$ orbital to the SOMO is proportional to the difference between these two values, and their similarity means that this contribution is very small (between 0 and

(18) McInnes, E. J. L.; Farley, R. D.; Rowlands, C. C.; Welch, A. J.; Rovatti, L.; Yellowlees, L. J. *J. Chem. Soc., Dalton Trans.* **1999**, 4203–4208.

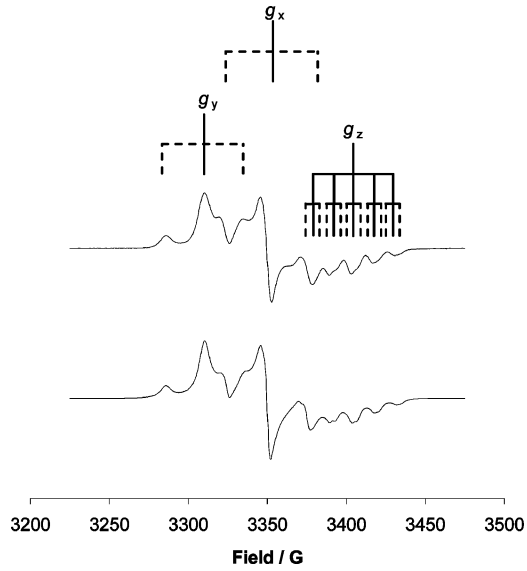

Figure 4. Experimental (top) and simulated (bottom) ESR spectra of $\mathbf{3}^-$, showing the location of the three g values, and coupling to ^{195}Pt (dashed lines) and ^{14}N (solid line, g_z only).

1%); the ESR spectra imply that the overwhelming metal contribution to the SOMO is from the $6p_z$ orbital. By comparison the anions [Pt(MesBIAN)(SS)]$^-$, where SS is a dithiolate ligand,[11] have a much larger difference between A_y and A_x and a much smaller difference between A_y and A_z, implying more d-orbital and less p-orbital contribution to the SOMO {e.g., for [Pt(MesBIAN)(mnt)]$^-$ (mnt = 1,2-maleonitriledithiolate), $A_y = -71$, $A_x = -90$, $A_z = -55 \times 10^{-4}$ cm^{-1}}, although the total metal contribution to the SOMO is still around 10%.[11] The differences may be due to the differences between the π-acceptor dithiolate ligands and the π-donor acetylides; the former lower the energy of the $5d_{yz}$ orbital, allowing it to overlap well with the MesBIAN orbitals that predominantly form the SOMO, whereas the latter raise the energy of the $5d_{yz}$ orbital and reduce its contribution to the SOMO.

The stability of the reduced species $\mathbf{1}^-$−$\mathbf{5}^-$ and the presence of the infrared active carbon−carbon triple bonds meant that it was possible to obtain IR spectra of these anions (Table 5), generated by reduction of dichloromethane solutions of the appropriate neutral species with decamethylcobaltocene. The IR spectra of the neutral compounds **1**−**5** show a characteristic broad band centered at about 2126 cm^{-1}, which results from the overlap of the symmetric and antisymmetric ν(C≡C) stretching vibrations. The position of this band is virtually independent of the acetylide involved. Upon reduction, ν(C≡C) shifts to lower energies by 15 to 26 cm^{-1} and increases considerably in intensity (Figure 5), indicating an increase in the amount of backbonding into the antibonding orbitals of the triple bonds consistent with the calculated nature of the LUMO (below). In some cases a third, weak, IR band was observed, probably because of Fermi resonance.

Oxidative Addition Reaction. Many platinum(II) compounds with carbon ligands will oxidatively add reagents such as diiodine to form stable platinum(IV) species.[19] We investigated the oxidation of **4** by diiodine in dichloromethane as a representative example. The reaction as followed by NMR showed a very clean process, involving the generation of a single intermediate species which then decayed to form the final product. Upon performing the reaction on a preparative scale, the product was identified as [Pt(MesBIAN)I_2] **6**. It is likely that this product is formed by oxidative addition of the iodine to **4** and subsequent reductive coupling and elimination of the two alkyne ligands as a diyne (Scheme 2).[20] This proposition is supported by the isolation of the diyne from the reaction mixture and its identification by ^{1}H NMR spectroscopy and elemental analysis.

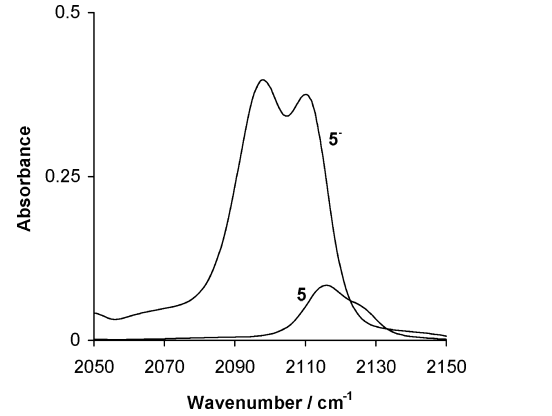

Figure 5. IR spectra of **5** and $\mathbf{5}^-$, recorded in CH_2Cl_2 solution at room temperature.

Scheme 2. Formation of **6** by Oxidative Addition of Iodine to **4** Followed by Reductive Elimination of a Diyne (R = p-C_6H_5)

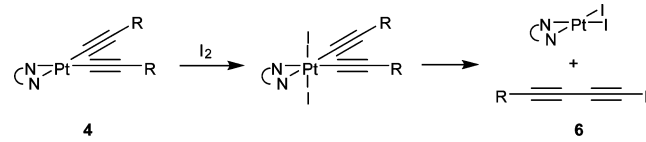

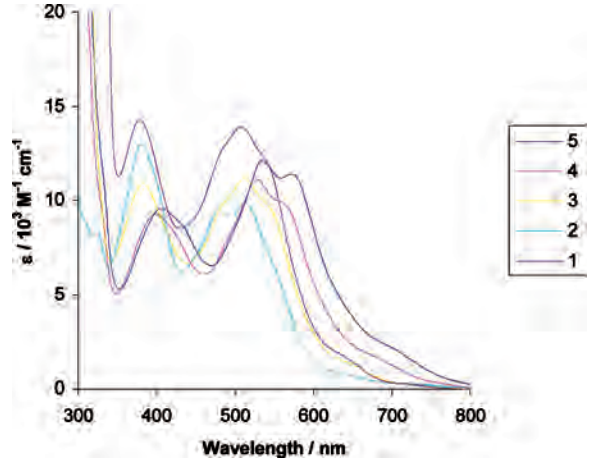

Figure 6. Absorption spectra of **1**−**5** in CH_2Cl_2 at room temperature.

Electronic Absorption Spectroscopy. The absorption spectra of **1**−**5** are detailed in Table 4 and shown in Figure 6. The high energy absorption bands observed in the range 250−300 nm are due to intraligand π-π^* transitions. There are two further main absorption band envelopes, one at 370−420 nm and a second between 500 and 700 nm ($\varepsilon \approx$ 10000−12000 M^{-1} cm^{-1}). The latter shows some vibrational structure, which is best resolved for **2** and **5**, with the

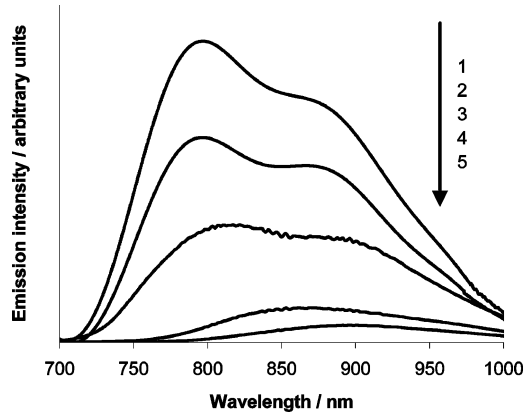

Figure 7. Emission spectra of **1**−**5** in degassed CH_2Cl_2 solution at room temperature (RT), normalized by the value of the quantum yields, under 514.5 nm excitation with a CW Ar ion laser. For clarity of presentation, the spectra of **3**−**5** are multiplied by 2.5.

difference between the components being between 1420 and 1455 cm^{-1}. These values match the vibrational frequencies of the coordinated MesBIAN ligand previously determined for [Pt(MesBIAN)Cl_2] by Raman spectroscopy.[11] We therefore assign these bands to a vibrational progression within the same electronic transition and take this fact as an indication of MesBIAN orbital participation in this electronic transition. The energy of the absorption band decreases with an increase of the electron donor capability of the arylacetylide ligands, indicating acetylide ligand involvement in the electronic transition in question.

In concentrated solutions, it is also possible to discern very weak absorption transitions on the low energy side of the main absorption band, in the range 720−790 nm (ε < 400 M^{-1} cm^{-1}, Table 4), which we assign to the corresponding singlet−triplet transitions, facilitated by the presence of the heavy atom.

Emission Spectroscopy and Singlet Oxygen Generation. Compounds **1**−**5** are luminescent in degassed dichloromethane solution at room temperature (Figure 7 and Table 4). The emission maxima are in the range 780 to 900 nm, and emission lifetimes are in the order of several tens of nanoseconds. By comparison to platinum−acetylide complexes with 1,10-phenanthroline or 2,2′-bipyridine ligands and their derivatives, which typically emit in the range 450−600 nm,[6,21−25] use of the strongly accepting MesBIAN ligand considerably decreases the emission energies, yielding emission in the NIR range. Consequently, emission quantum yields are of the order of 0.5% or less (Table 4), and emission lifetimes are lower than those of most of the [Pt(diimine)(acetylide)$_2$] compounds that emit in the visible region. It is noteworthy that the emission lifetimes of **1**−**5** are still remarkably long for NIR emitters. The lifetime of the excited states of **1**−**5** is sufficiently long to generate singlet oxygen upon irradiation of their solution in dichloromethane with 355 nm laser light. The yield of $^1O_2$, determined as described previously,[26] is 10% for **1** and **3** and 7% for **4** and **5**.

It has been reported previously that the use of more electron accepting diimine derivatives leads to a decrease in emission yield and lifetime.[8] This trend is clearly seen for [Pt(diimine)(−C≡C−C_6H_4−CH_3)$_2$] compounds, where emission energies, quantum yields (ϕ) and lifetimes (τ) decrease systematically with an increase of the diimine acceptor capability along the series of diimines = 4,4′-*tert*-butyl-2,2′-bipyridine (λ_{max} = 570 nm, ϕ = 0.113, τ = 800 ns), 4,4′-C(O)NEt_2-2,2′-bipyridine (λ_{max} = 642 nm, $\phi = 7.0 \times 10^{-3}$, τ = 103 ns), 4,4′-C(O)OEt-2,2′-bipyridine (λ_{max} = 670 nm, $\phi = 4.6 \times 10^{-3}$, τ = 20 ns).[8] The photophysical properties of **5** (λ_{max} = 905 nm, $\phi = 9 \times 10^{-5}$, τ = 8 ns) clearly follow this trend. The dependence on the nature of the diimine indicates the involvement of MesBIAN-localized orbital(s) in the emissive excited state.

The emission spectra for the compounds **1**−**3** are structured, comprising two bands having a ∼1360 cm^{-1} energy difference. This value is typical for a vibrational progression associated with diimine vibrational modes, is similar to that reported previously for some other platinum(II)−diimine−acetylide complexes,[8,21,27] and is characteristic of diimine ligand involvement in the emissive excited state.[28−30] Two overlapping bands were also resolved by Gaussian deconvolution of the spectra of **4** and **5** (Table 4). A good match between the emission excitation spectra and the absorption spectra of **1**−**5** confirms that in each case emission originates from the parent compound.

Along the series **1**−**5**, the emission maxima, lifetimes, and quantum yields decrease systematically with an increase of the acetylide ligand donor capability. The emission energy depends linearly on the difference between the reduction and oxidation potentials of **1**−**5**, indicating involvement of both diimine- and acetylide-based orbitals in the emissive excited state. At the same time, the trends in quantum yields and lifetimes follow the trend in emission energies. Such clear trends indicate that an excited state of the same origin is responsible for the emission from all the compounds **1**−**5**.

(19) Rendina, L. M.; Puddephatt, R. J. *Chem. Rev.* **1997**, *97*, 1735–1754.
(20) James, S. L.; Younus, M.; Raithby, P. R.; Lewis, J. *J. Organomet. Chem.* **1997**, *543*, 233–235.
(21) Wadas, T. J.; Lachicotte, R. J.; Eisenberg, R. *Inorg. Chem.* **2003**, *42*, 3772–3778.
(22) Wadas, T. J.; Chakraborty, S.; Lachicotte, R. J.; Wang, Q. M.; Eisenberg, R. *Inorg. Chem.* **2005**, *44*, 2628–2638.
(23) Chan, S. C.; Chan, M. C. W.; Wang, Y.; Che, C. M.; Cheung, K. K.; Zhu, N. Y. *Chem.*−*Eur. J.* **2001**, *7*, 4180–4190.
(24) Hua, F.; Kinayyigit, S.; Cable, J. R.; Castellano, F. N. *Inorg. Chem.* **2005**, *44*, 471–473.
(25) McGarrah, J. E.; Eisenberg, R. *Inorg. Chem.* **2003**, *42*, 4355–4365.
(26) Shavaleev, N. M.; Adams, H.; Best, J.; Edge, R.; Navaratnam, S.; Weinstein, J. A. *Inorg. Chem.* **2006**, *45*, 9410–9415.
(27) Siemeling, U.; Bausch, K.; Fink, H.; Bruhn, C.; Baldus, M.; Angerstein, B.; Plessow, R.; Brockhinke, A. *Dalton Trans.* **2005**, 2365–2374.
(28) Excimer formation is a common phenomenon for square-planar Pt(II) systems. In the case of Pt(MesBIAN) compounds, the difference in energies between the two bands forming the emission spectrum of **1**−**3** is typical for a vibrational progression and is much smaller than that reported previously for monomer/excimer formation in similar complexes, and the spectral shape does not depend on the concentration from 15 to 70 M. We therefore tend to attribute the emission spectrum observed under our experimental conditions to monomer emission, rather than to a combination of a monomer and an excimer emission. The lack of stacking under the concentrations used may also be attributed to the bulky mesityl groups of the MesBIAN ligand.
(29) Connick, W. B.; Geiger, D.; Eisenberg, R. *Inorg. Chem.* **1999**, *38*, 3264–3265.
(30) Ronson, T. K.; Lazarides, T.; Adams, H.; Pope, S. J. A.; Sykes, D.; Faulkner, S.; Coles, S. J.; Hursthouse, M. B.; Clegg, W.; Harrington, R. W.; Ward, M. D. *Chem.*−*Eur. J.* **2006**, *12*, 9299–9313.

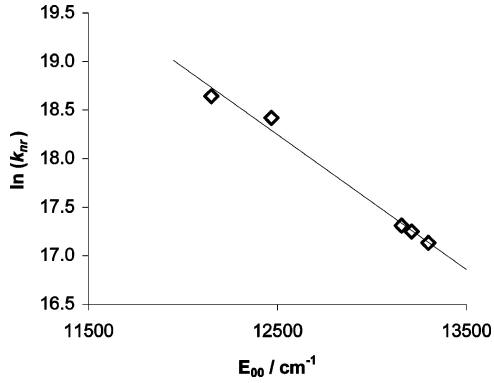

Figure 8. Plot of ln(k_{nr}) vs E_{00} for **1**−**5** in dichloromethane at RT.

The emission maxima of **1**−**5** are close in energy to the weak, lowest energy band (e.g., 719 and 786 nm respectively for **1**, Table 4) in the absorption spectrum. This small Stokes shift supports further the triplet assignment of the weak low-energy absorption band and points to the triplet character of the emissive excited state. Generation of singlet oxygen by **1**−**5** is also consistent with the triplet nature of their lowest excited state. The rate constant of nonradiative decay, k_{nr}, of the excited state (Table 4) increases systematically as the acetylide ligand electron donating capability increases, contributing to the observed decrease of the emission quantum yields, energies, and lifetimes in accord with the energy gap law.[31] The correlation between ln(k_{nr}) and the energy of the zero-zero transition E_{00} can be presented as $\ln(k_{nr}) = a - (\gamma_0/\hbar\omega_m)E_{00}$, where $\gamma_0 = \ln(E_{00}/S_m\hbar\omega_m) - 1$. The term $\hbar\omega_m$ is the average medium-frequency vibrational mode coupled to the MMLL′CT transition, and S_m is the Huang−Rhys factor, which quantifies electronic-vibrational coupling. E_{00} has been estimated from the highest energy emission maximum and the lowest energy, weak absorption band in the UV/vis spectrum (Table 4). The slope of the linear correlation between ln(k_{nr}) and E_{00} (Figure 8) is -1.4×10^{-3} cm^{-1}, which is close to that reported previously[8] for a series of [Pt(diimine)(−C≡C−C_6H_4−CH_3)$_2$] complexes (-1.18×10^{-3} cm^{-1}). Assuming that S_m equals 1, the experimentally observed slope can be used to calculate $\hbar\omega_m$ as 1120 cm^{-1}, which is in the range of diimine-localized modes. Interestingly, this means that the acetylide bond does not act as an acceptor mode in the nonradiative decay of the ^{3}MLL′CT state.

The data presented above indicate the involvement of both acetylide and MesBIAN orbitals in the emissive excited state. Taking into account the electrochemical and ESR data that showed the MesBIAN/Pt character of the SOMO in the radical anions **1**$^-$−**5**$^-$ (vide supra), the lowest electronic transition is assigned as mixed metal/ligand-to-ligand charge transfer in origin (MMLL′CT), from the metal-acetylide moiety to a diimine π^* orbital. Consistent with this assignment, the lowest absorption envelope shows negative solvatochromism; that is, a decrease in absorption energy with a decrease in solvent polarity. The slope of the linear correlation between the absorption maximum and the solvent parameter[32] for **5** is 0.24 eV, which is in the range typical for charge-transfer transitions.[32] Such an assignment is consistent with the assignment of the lowest absorption bands in the UV/vis spectra and with the results of theoretical calculations and TRIR spectroscopy discussed below.

TRIR Spectroscopy of 5. The presence of an infrared active C≡C bond in **1**−**5** allows for the application of TRIR spectroscopy to investigate further the nature and dynamics of their excited states; [Pt(MesBIAN)(−C≡C−C_6H_4−CH_3)$_2$] **5**, which possesses the most short-lived excited state among **1**−**5**, was studied as a representative example. TRIR, a combination of UV flash photolysis and fast IR detection, has been widely used as a powerful probe of the nature of the excited states of coordination compounds,[33−36] including Pt(II) chromophores.[7,8,37−43]

Both picosecond and nanosecond TRIR have been utilized. The experiments were performed in three separate spectral windows, covering the total range between 1790 and 2180 cm^{-1}; it should be noted that the spectral range between 1790 and 1950 cm^{-1} has not previously been investigated for platinum(II)−diimine−acetylide compounds. In this spectral range, the ground-state IR spectrum of **5** in CH_2Cl_2 at RT is dominated by an asymmetric IR band due to ν(C≡C), with a maximum at 2115 cm^{-1} (Figure 9a). Lorentzian deconvolution of this IR band (Figure 9a) reveals the presence of two overlapping bands, at 2124 and 2115 cm^{-1}, as expected for a bis(acetylide) compound. These ν(C≡C) band positions are practically identical to those reported for [Pt(4,4′-X_2-bpy)(−C≡C−C_6H_4−CH_3)$_2$],[6] indicating that the diimine ligand has little effect on the electron density of the −C≡C− bond in the electronic ground state.

Both 400 nm, 150 fs excitation, and 355 nm, 0.6 ns excitation lead to identical TRIR spectra, shown in Figure 10 for the nanosecond time scale, and in the ESI for the picosecond time scale. A bleach of the ground-state absorbance at 2115 cm^{-1} is observed, with the concomitant formation of new, very intense, transient bands centered at 2028 and 1820 cm^{-1}.

(31) Caspar, J. V.; Meyer, T. J. *J. Phys. Chem.* **1983**, *87*, 952.
(32) Cummings, S. D.; Eisenberg, R. *J. Am. Chem. Soc.* **1996**, *118*, 1949–1960.
(33) Schoonover, J. R.; Bignozzi, C. A.; Meyer, T. J. *Coord. Chem. Rev.* **1997**, *165*, 239–266.
(34) Schoonover, J. R.; Strouse, G. F. *Chem. Rev.* **1998**, *98*, 1335–1356.
(35) Butler, J. M.; George, M. W.; Schoonover, J. R.; Dattelbaum, D. M.; Meyer, T. J. *Coord. Chem. Rev.* **2007**, *251*, 492–514.
(36) George, M. W.; Turner, J. J. *Coord. Chem. Rev.* **1998**, *177*, 201–217.
(37) Weinstein, J. A.; Grills, D. C.; Towrie, M.; Matousek, P.; Parker, A. W.; George, M. W. *Chem. Commun.* **2002**, 382–383.
(38) Weinstein, J. A.; Blake, A. J.; Davies, E. S.; Davis, A. L.; George, M. W.; Grills, D. C.; Lileev, I. V.; Maksimov, A. M.; Matousek, P.; Mel'nikov, M. Y.; Parker, A. W.; Platonov, V. E.; Towrie, M.; Wilson, C.; Zheligovskaya, N. N. *Inorg. Chem.* **2003**, *42*, 7077–7085.
(39) Smith, G. D.; Hutson, M. S.; Lu, Y.; Tierney, M. T.; Grinstaff, M. W.; Palmer, R. A. *Appl. Spectrosc.* **2001**, *55*, 637–642.
(40) Dougherty, T. P.; Heilweil, E. J. *Chem. Phys. Lett.* **1994**, *227*, 19–25.
(41) Hamm, P.; Ohline, S. M.; Zinth, W. *J. Chem. Phys.* **1997**, *106*, 519–529.
(42) Marks, S.; Cornelius, P. A.; Harris, C. B. *J. Chem. Phys.* **1980**, *73*, 3069–3081.
(43) Towrie, M.; Grills, D. C.; Dyer, J.; Weinstein, J. A.; Matousek, P.; Barton, R.; Bailey, P. D.; Subramaniam, N.; Kwok, W. M.; Ma, C. S.; Phillips, D.; Parker, A. W.; George, M. W. *Appl. Spectrosc.* **2003**, *57*, 367–380.

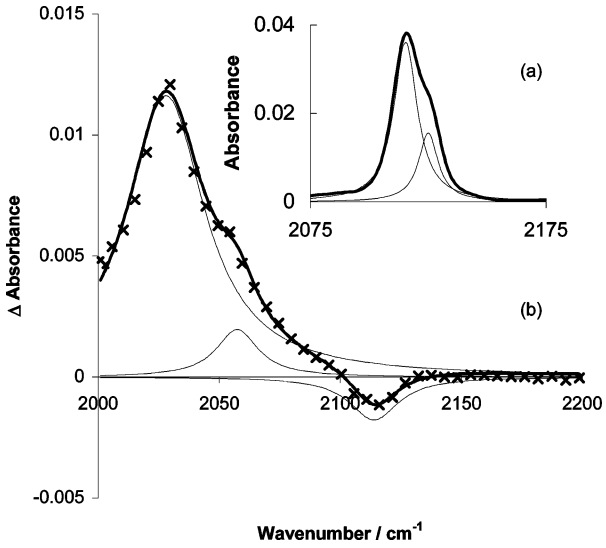

Figure 9. (a) Ground-state FTIR spectrum of **5** in CH_2Cl_2. The Lorentzian fit to the spectrum (bold) shows bands at 2124 and 2115 cm^{-1} due to the symmetric and antisymmetric combinations of the CC triple bond vibrations. (b) TRIR spectrum of **5**, at 100 ps after a 400 nm, 150 fs laser excitation pulse (×). The bold line represents a multi-Lorentizan fit to the spectrum, resolving the bands at 2028 and 2057 cm^{-1} and the bleach at 2124 cm^{-1} in the excited state (fine lines).

The TRIR spectra display several intriguing features:

(i) A shift to lower energies of ν(C≡C) upon generation of the excited state;

(ii) Transient C≡C bands of much higher intensity than those of the ground state;

(iii) A new very broad (ca. 110 cm^{-1} full width at half maximum (fwhm)) transient band at 1820 cm^{-1}.

The spectra at all time delays were fitted assuming a Lorentzian band shape (an example of the fit is given in Figure 9b). The transient band centered at 2028 cm^{-1} (with a weaker second band at 2057 cm^{-1}) probably corresponds to the acetylide vibrations in the excited state. A large negative shift in the energy of the acetylide stretching vibrations (ca. −87 cm^{-1}) is indicative of a decrease of electron density in the π-bonding orbital of the C≡C moiety, consistent with a transfer of electron density away from the acetylide ligands upon formation of the ^{3}MMLL′CT excited state. The much greater intensities of the transient bands compared to those of the ground state imply that there is a substantial increase in the dipole moment associated with the vibrations in question upon generation of the excited state.

Given a platinum-acetylide based HOMO, and the predominantly MesBIAN-based LUMO, the broad band at 1820 cm^{-1} could originate from either an "oxidized" platinum−acetylide moiety or from a MesBIAN moiety "reduced" while in the excited state. The lack of any intense bands in the region 1700−1950 cm^{-1} in the spectrum of the chemically generated radical anion $[Pt(MesBIAN)(-C{\equiv}C-C_6H_4-CH_3)_2]^-$ **5**$^-$, which according to ESR data contains unpaired electron density localized mainly on the coordinated MesBIAN ligand, rules out a MesBIAN-anion localization of the 1820 cm^{-1} vibration in the excited state. Thus, both 2028 and 1820 cm^{-1} vibrations detected in the excited state are likely to be largely localized on the platinum−acetylide moiety.

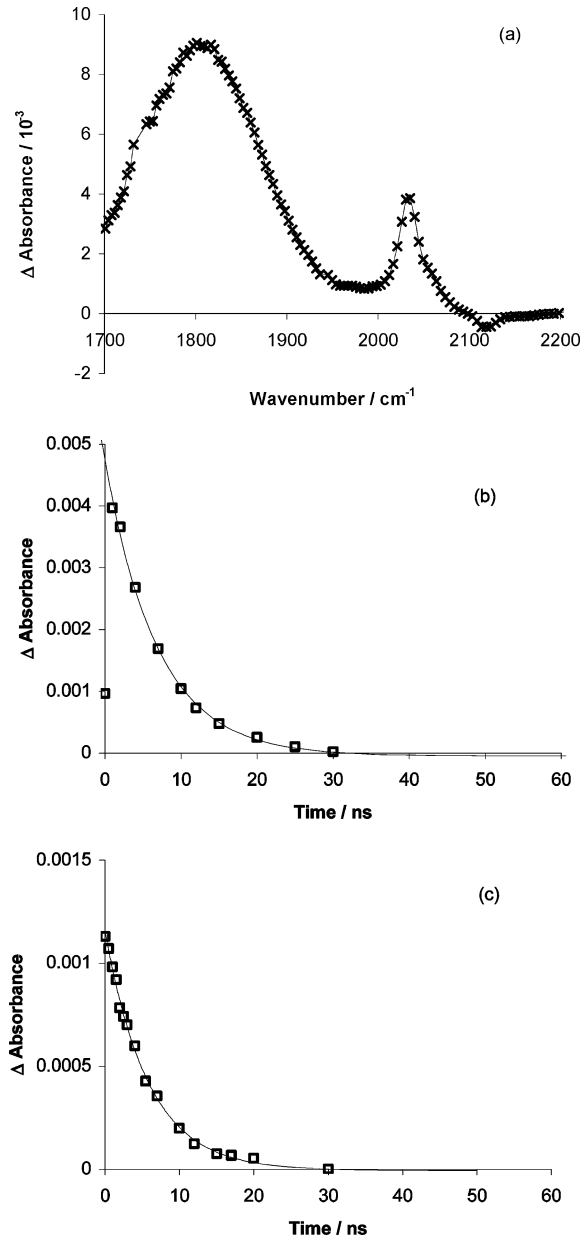

Figure 10. Nanosecond TRIR data for **5** at RT. (a) Infrared spectrum of 1 mM solution of **5** in THF, recorded 2 ns after the 400 nm, ∼150 fs laser pulse. (b) Kinetics at 1820 cm^{-1} (□), the solid line representing a monoexponential fit to the data with $\tau = 6.5 \pm 0.5$ ns. (c) Kinetics at 2058 cm^{-1} (□), the solid line representing a monoexponential fit to the data with $\tau = 5.9 \pm 0.5$ ns.

We therefore propose that in the charge-transfer excited state of **5** a general delocalization of electron density away from both acetylide ligands to the MesBIAN ligand takes place. This reduces the bond order of both C≡C bonds (as one electron is removed from a molecular orbital containing both C≡C bonding orbitals), while concomitantly increasing the bond order of each Pt−C and C−Aryl bond, creating two partially cumulated Pt═C═C═Aryl units. The vibrations observed are then the symmetric and antisymmetric combinations of these stretches, which because of the nature of the depopulated HOMO may also include contributions from the vibrations of the aryl units.

Support for this hypothesis comes from the TRIR spectra reported for the triplet excited state of *trans*-[(Ph≡Ph≡)$_2$-

$Pt(PBu_3)$].[7] In this case, promotion to the triplet state from the ground state is accompanied by bleaching of the ground-state triple bond band at 2090 cm^{-1} and of a weak 1600 cm^{-1} band due to the aryl ring. The excited-state spectrum features bands at 2040 cm^{-1} and 1820 cm^{-1}, the latter being extremely broad (ca. 80 cm^{-1} fwhm) and about three times more intense than the 2040 cm^{-1} band. These features are very similar to those observed in the TRIR spectra of **5** (Figures 9 and 10).

On the nanosecond time scale, the whole TRIR spectrum decays simultaneously, with the lifetimes of the monoexponential decay for the 1820 cm^{-1} (6.9 ± 1.0 ns) and 2028 cm^{-1} (5.9 ± 1.0 ns) transient bands being virtually the same within experimental error, and matching the rate of the parent bleach recovery. This fact indicates that the transient spectrum as a whole is characteristic of one electronic excited state. The lifetime of this excited state as determined from TRIR measurements (ca. 1 mM concentration) is very close to that determined in the time-resolved emission experiments {8.0 (±0.8) ns, 10^{-5} M} on **5**, again indicating that the TRIR spectrum corresponds to the emissive excited state. The slightly shorter lifetime determined in the TRIR experiments could be due to the well-documented self-quenching of platinum(II) complexes in the excited state.[29]

While our results correspond well with the reported TRIR data for *trans*-[(Ph-≡-Ph-≡-)$_2$Pt(PBu_3)],[7] they differ from those for the complex [Pt(dbbpy)(−C≡C−C_6H_4−CH_3)$_2$].[8] In the latter, a shift of ν(C≡C) to higher energies by about +30 cm^{-1} upon formation of the excited state was reported, and the intensity of the transient band was comparable to that of the ground-state bleach. The contrasting appearance of the TRIR spectrum of **5** implies that the change in the diimine ligand has a profound effect on the nature of the excited state. The much stronger electron accepting capability of the MesBIAN ligand than of 2,2-bipyridine {[Pt(bipy)Cl_2] is reduced at −1.14 V versus SCE[18] whereas [Pt(MesBIAN)Cl_2] is reduced at −0.60 V}[10] may lead to a larger shift of electron density in platinum−MesBIAN complexes away from the triple bonds upon generation of the excited state. Thus, excitation of **5** depopulates the −C≡C− bonding orbital, weakening the bond and lowering the corresponding vibrational frequency. In contrast, the raising of ν(C≡C) upon excitation of [Pt(dbbipy)(−C≡C−C_6H_5−CH_3)$_2$] was attributed to excitation reducing platinum to acetylide back-bonding;[8] however, recent studies on the very similar complex [Pt(dbbpy)(−C≡C−C_6H_5)$_2$] agree with our hypothesis that the acetylide bonding orbital is depopulated upon excitation, rather than there being a reduction in platinum to acetylide π^* backbonding.[44] In principle, admixture of an intra-acetylide $^3\pi\pi^*$ excited state into the MMLL′CT excited state could also contribute to the negative shift of ν(C≡C) because of population of the π^*-antibonding orbital. However, for the MesBIAN compounds herein, the $^3\pi\pi^*$ state appears to be too high in energy in comparison with the MMLL′CT state to have significant influence.

The observed spectral profile for **5** was not concentration dependent over a concentration range from 2.5 mM to 46 mM. That the same TRIR profile was observed in THF and CH_2Cl_2 (shown in the Supporting Information) confirms that the observed transient features arise from the system investigated and are not due to any artifacts associated with the solvent. No deviations from Buger−Beer's law have been observed for the ground state of the complex up to a 70 mM concentration.

Picosecond TRIR Spectroscopy of 5. Picosecond TRIR spectra were recorded at several pump−probe delays, between 1 and 2500 ps. Upon excitation with a 400 nm, 150 fs laser pulse an instantaneous bleaching of the parent absorption was observed, concomitant with the formation of intense new bands at about 2028 and 1820 cm^{-1}. The position and the shape of the 2028 cm^{-1} transient band is time-dependent on the picosecond time scale, with the band position shifting to higher frequencies and the bandwidth decreasing with time (Figure 11a). Such behavior is typical of an early relaxation process associated with the decay of the vibrationally "hot" excited state initially formed upon laser excitation.[7,37,40−42,45−50]

The kinetic traces obtained using multi-Lorentzian curve fitting of the spectra at each time delay are shown in Figure 11. The spectral fitting was achieved by fixing the position and fwhm of the ground-state bleach, as determined from the FTIR spectrum. The monoexponential fit of the difference between the position of the vibrationally "hot" band and the vibrationally "cold", relaxed ν(C≡C) band of **5** yields the lifetime of vibrational relaxation of 13.0 ± 2.0 ps (Figure 11b). A value of 15.0 ± 2.0 ps, virtually identical within experimental error, was obtained from a monoexponential decay of the fwhm of this band to the "relaxed" fwhm (Figure 11c). The similarity indicates that there is little involvement of the solvent in the relaxation process.[46] The average 14 ps lifetime obtained for vibrational cooling of ν(C≡C) in **5** is at the lower limit of the values reported for vibrational cooling rates of metal carbonyls, but considerably longer than that of organic reporters (2−5 ps).[35,51] A similar rate of vibrational relaxation, 8 ps, has been reported for a carbonyl group attached to a platinum(II) center in [Pt(thpy)(mts)(CO)] {thpy = 2-thienylpyridine, mts = methylthiosalicylate}.[52] To the best of our knowledge, the current work is the first observation of the vibrational relaxation of an acetylide group attached to a metal center.

(44) Hua, F.; Kinayyigit, S.; Rachford, A. A.; Shikhova, E. A.; Goeb, S.; Cable, J. R.; Adams, C. J.; Kirschbaum, K.; Pinkerton, A. A.; Castellano, F. N. *Inorg. Chem.* **2007**, *46*, 8771–8783.

(45) Zalis, S.; Farrell, I. R., Jr *J. Am. Chem. Soc.* **2003**, *125*, 4580.

(46) Asbury, J. B.; Wang, Y.; Lian, T. *Bull. Chem. Soc. Jpn.* **2002**, *75*, 973.

(47) Steinhurst, D. A.; Baronavski, A. P.; Owrutsky, J. C. *Chem. Phys. Lett.* **2002**, *361*, 513.

(48) Wang, Y. Q.; Asbury, J. B.; Lian, T. Q. *J. Phys. Chem. A* **2000**, *104*, 4291.

(49) Damrauer, N. H.; McCusker, J. K. *J. Phys. Chem. A* **1999**, *103*, 8440.

(50) Henry, W.; Coates, C. G.; Brady, C.; Ronayne, K. L.; Matousek, P.; Towrie, M.; Botchway, S. W.; Parker, A. W.; Vos, J. G.; Browne, W. R.; McGarvey, J. J. *J. Phys. Chem. A* **2008**, *112*, 4537–4544.

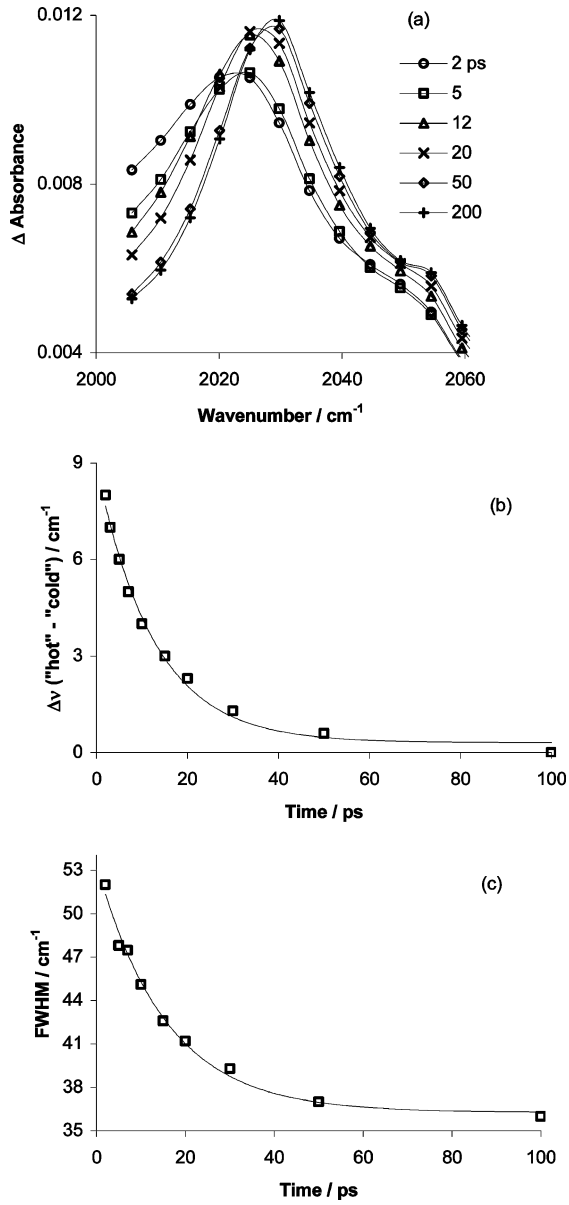

Figure 11. (a) Picosecond dynamics of the shape of the transient 2028 cm^{-1} band recorded in the TRIR spectrum of **5** in CH_2Cl_2 from 2 to 200 ps after 400 nm, 150 fs laser excitation. (b) Kinetics of the shift of the position of the transient band; the solid line represents a monoexponential fit to the data with $\tau = 13.0 \pm 2.0$ ps. (c) Kinetics of the change of the fwhm of the transient band; the solid line represents a monoexponential fit to the data with $\tau = 15.0 \pm 2.0$ ps.

Computational Studies

To further probe the nature and structure of the excited state of **1**−**5** we have performed DFT calculations using the B3LYP functional to model **5** in both the ground-state singlet (henceforth **5s**) and the lowest excited-state triplet (**5t**) states. For singlet calculations, three different geometries were employed; one with both phenyl rings of the acetylide ligands perpendicular to the diimine system (henceforth $\mathbf{5s}_{\perp}$), one where they were coplanar with it ($\mathbf{5s}_{\parallel}$), and one with one ring perpendicular and one coplanar (**5sx**). The latter is the geometry obtained if the crystallographically determined structure described above is used as the starting point for the geometry optimization, rather than restricting the complex to the C_{2v} symmetry used in the first two cases; however, it is $\mathbf{5s}_{\parallel}$ that has the lowest energy of the three geometries. For the triplet state, an optimization from the crystal structure geometry yields a model with both rings planar ($\mathbf{5t}_{\parallel}$) which is approximately 1.29 eV (29.70 kcal mol^{-1}) higher in energy than the ground singlet state; the geometry with both rings perpendicular ($\mathbf{5t}_{\perp}$) lies a further 0.4 eV (9.25 kcal mol^{-1}) higher in energy (Table 6). In each case frequency calculations confirmed that the structures were minima, and the PCM formalism was employed to model a dichloromethane solvent continuum.

Table 6. Energies and Important Computed Bond Lengths [Å] for **5**

	relative energy					
	kcal mol^{-1}	eV	Pt−C	Pt−N	C≡C	C−Ph
			Singlet Structures			
$\mathbf{5s}_{\perp}$	2.54	0.110	1.956	2.145	1.227	1.430
$\mathbf{5s}_{\parallel}$	0	0	1.953	2.141	1.228	1.429
5sx	1.48	0.064	1.952	2.144	1.228	1.428
			1.955	2.147	1.227	1.430
			Triplet Structures			
$\mathbf{5t}_{\perp}$	38.95	1.689	1.941	2.105	1.238	1.414
$\mathbf{5t}_{\parallel}$	29.70	1.288	1.942	2.104	1.238	1.414

The calculated bond lengths of **5** agree reasonably well (Table 6) with the crystallographic structure (Table 2), and the values vary little with the geometry used. The crystallographically observed torsion angles of the tolyl rings are not reproduced correctly, which is unsurprising for a peripheral group which may be conformationally mobile in the gas phase and in fluid solution. The calculated geometries overestimate the Pt−N distances (2.14 Å vs. 2.07 Å), but predict a Pt−C distance of 1.95 Å, between the two experimental values (1.94 and 1.96 Å). The calculated C≡C length of 1.23 Å is also slightly longer than the experimental value (1.20 Å).

By comparison with the singlet geometries, the computed triplet structures of **5** show only small changes to the bond lengths of the Pt−C≡C−Ph unit consistent with the acquisition of a slight degree of cumulenic structure. Thus, the Pt−C distance decreases by 0.01 Å to 1.94 Å, the −C≡C− bond length increases by 0.01 Å to 1.24 Å, and the C−Ph distance decreases by 0.015 Å to 1.414 Å. These changes are significantly smaller than those previously calculated for *trans*-{$Pt(PMe_3)_2(-C\equiv C-Ph)_2$},[53] in which the C≡C bond length increases by 0.043 Å and the C−Ph distance decreases by 0.068 Å on moving from singlet to triplet. We attribute this difference to the fact that in *trans*-{$Pt(PMe_3)_2(-C\equiv C-Ph)_2$} both depopulation of the HOMO and population of the LUMO contribute to cumulenic structure, in contrast to the situation for **5** where only HOMO depopulation has this effect. Also, because of symmetry breaking in the excited state of *trans*-{$Pt(PMe_3)_2(-C\equiv C-Ph)_2$}, the changes observed are localized only on one −C≡C−Ph group. Larger differences between the singlet and triplet

(51) Liard, D. J.; Busby, M.; Matousek, P.; Towrie, M.; Vlcek, A. *J. Phys. Chem. A* **2004**, *108*, 2363–2369.
(52) Kovelenov, Y. A.; Blake, A. J.; George, M. W.; Matousek, P.; Mel'nikov, M. Y.; Parker, A. W.; Sun, X. Z.; Towrie, M.; Weinstein, J. A. *Dalton Trans.* **2005**, 2092.
(53) Cooper, T. M.; Krein, D. M.; Burke, A. R.; McLean, D. G.; Rogers, J. E.; Slagle, J. E. *J. Phys. Chem. A* **2006**, *110*, 13370–13378.

Table 7. Calculated Symmetry and Percentage Compositions of Orbitals Involved in Low-Energy UV-visible Transitions in Models of **5**[a]

model		orbital	178	179	180	181 (HOMO)	182 (LUMO)	183
$\mathbf{5s}_{\perp}$	symmetry		b_1	a_2	b_2	a_1	b_1	a_2
	energy/eV		−6.05	−5.77	−5.42	−5.25	−3.09	−2.37
	composition (%)	Pt	43	40	1	23	7	1
		MesBIAN	11	9	3	3	89	99
		π_1	19	21	21	16	1	0
		π_2	19	21	21	16	1	0
$\mathbf{5s}_{\parallel}$	symmetry		b_2	a_1	b_1	a_2	b_1	a_2
	energy/eV		−6.30	−5.96	−5.51	−5.24	−3.11	−2.36
	composition (%)	Pt	3	38	22	22	7	0
		MesBIAN	69	6	9	3	88	99
		π_1	12	23	15	18	1	0
		π_2	12	23	15	18	1	0
5sx	energy/eV		−6.14	−5.93	−5.33	−5.31	−3.09	−2.36
	composition (%)	Pt	21	40	23	16	7	0
		MesBIAN	10	11	4	3	88	99
		π_1	54	1	31	1	1	0
		π_2	2	37	3	35	1	0

[a] MesBIAN includes all the atoms of this ligand, and π_1 and π_2 refer to the two atoms of each carbon−carbon triple bond. In the model **5sx** where the two rings are approximately perpendicular to each other, π_1 is the triple bond of the ligand containing an in-plane tolyl ring, and π_2 is the triple bond of the ligand with a perpendicular ring.

geometries of **5** are seen in areas where both depopulation of the HOMO and population of the LUMO affect the bond lengths, occurring mainly around the MesBIAN ligand because of the location of the LUMO; for example, the Pt−N distances reduce by 0.037 Å, from 2.141 Å in $\mathbf{5s}_{\parallel}$ to 2.104 Å in $\mathbf{5t}_{\parallel}$.

A frequency calculation on $\mathbf{5s}_{\parallel}$ (singlet geometry, both rings parallel) predicted ν(C≡C) stretching frequencies of 2216 and 2195 cm^{-1} for the symmetric and antisymmetric modes, respectively. Applying an empirical scaling factor of 0.96 (which is equal to that applied in other studies)[54] reduces these values to 2127 and 2107 cm^{-1}, which compare well with the experimental values of 2124 and 2115 cm^{-1}. Similar values were calculated for $\mathbf{5s}_{\perp}$ (2224 and 2208 cm^{-1}) and **5sx** (2212 and 2192 cm^{-1}). The triplet state calculations shed light upon the experimentally observed IR spectrum of the excited state. For $\mathbf{5t}_{\parallel}$ (triplet state, both rings parallel), a band for a symmetric mode is predicted at 2150 cm^{-1}; this is accompanied by an asymmetric mode at 2013 cm^{-1} with twenty times the intensity. Scale factors of 0.94 and 0.90 respectively are required to convert these calculated values to the experimental frequencies (2028 and 1820 cm^{-1}). For $\mathbf{5t}_{\perp}$, the calculated frequencies are 2159 and 1942 cm^{-1}, the latter having eighteen times the intensity. In this case, a single scale factor of 0.94 would convert both calculated frequencies to the experimental values. Visualization of the vibrations in GAUSSVIEW[55] demonstrates that the bands predicted at 2028 and 1820 cm^{-1} correspond to the symmetric and antisymmetric combinations, respectively, of the same vibrations and that they are delocalized across the entire Ar−C≡C−Pt−C≡C−Ar moiety. No other vibrations were calculated in the range 1650 to 3000 cm^{-1}.

We note that only two bands are predicted in the triple-bond region of the TRIR spectrum of the triplet state, whereas in the experimental spectrum (Figure 10), as well as the very strong bands at 1820 and 2028 cm^{-1}, a shoulder at 2057 cm^{-1} was deconvoluted (Figure 9b). The reason for the observation of three (rather than two) bands remains unclear, although combination bands with an enhanced intensity because of Fermi coupling as observed in the spectra of some of the anions would offer one explanation. The close proximity of the Fermi band in the spectrum of $\mathbf{5}^-$ (at 2049 cm^{-1}) to the average position of the two deconvoluted components (2042 cm^{-1}) suggests that an interaction in the excited state is possible, but the assignment of the origin of particular band(s) to Fermi resonance is very difficult to prove experimentally in such complex systems. It has been reported previously that the calculations of the type performed here cannot predict vibrational bands that are due to Fermi resonance.[56,57]

Modeling the transitions in the UV−visible spectrum with TD-DFT was more dependent on model geometry than modeling of the IR spectra. For the singlet models $\mathbf{5s}_{\perp}$ and $\mathbf{5s}_{\parallel}$ the calculations show that within the triple bond of a coordinated acetylide ligand, the π-bonding orbital perpendicular to the plane of the aryl ring (i.e., composed of local p_z orbitals, and henceforth $\pi_{\perp}$) is higher in energy than the π-bonding orbital lying within this plane ($\pi_{\parallel}$). The two highest-energy occupied MOs are the out-of- and in-phase combinations of $\pi_{\perp}$-orbitals (Figure 12), and the two below are the combinations of $\pi_{\parallel}$-orbitals. The electron density located on the metal in these orbitals is between 0 and 43%, and on the two carbon atoms of each π-system between 0 and 54% (Table 7). The LUMO and LUMO+1 are always based largely (88−99%) upon the π-system of the MesBIAN ligand, and their energy does not vary significantly with the orientation of the ligands.

As we have found previously in the case of platinum−MesBIAN compounds with dithiolate co-ligands,[11] the

(54) Minaev, B.; Jansson, E.; Lindgren, M. *J. Chem. Phys.* **2006**, *125*, 094306.
(55) Dennington, R., II; Keith, T.; Millam, J. *GaussView*, Version 4.1; Semichem, Inc.: Shawnee Mission, KS, 2007.
(56) Devlin, F. J.; Stephens, P. J. *J. Phys. Chem. A* **1999**, *103*, 527–538.
(57) Autrey, D.; Yang, J.; Laane, J. *J. Mol. Struct.* **2003**, *661−662*, 23–32.

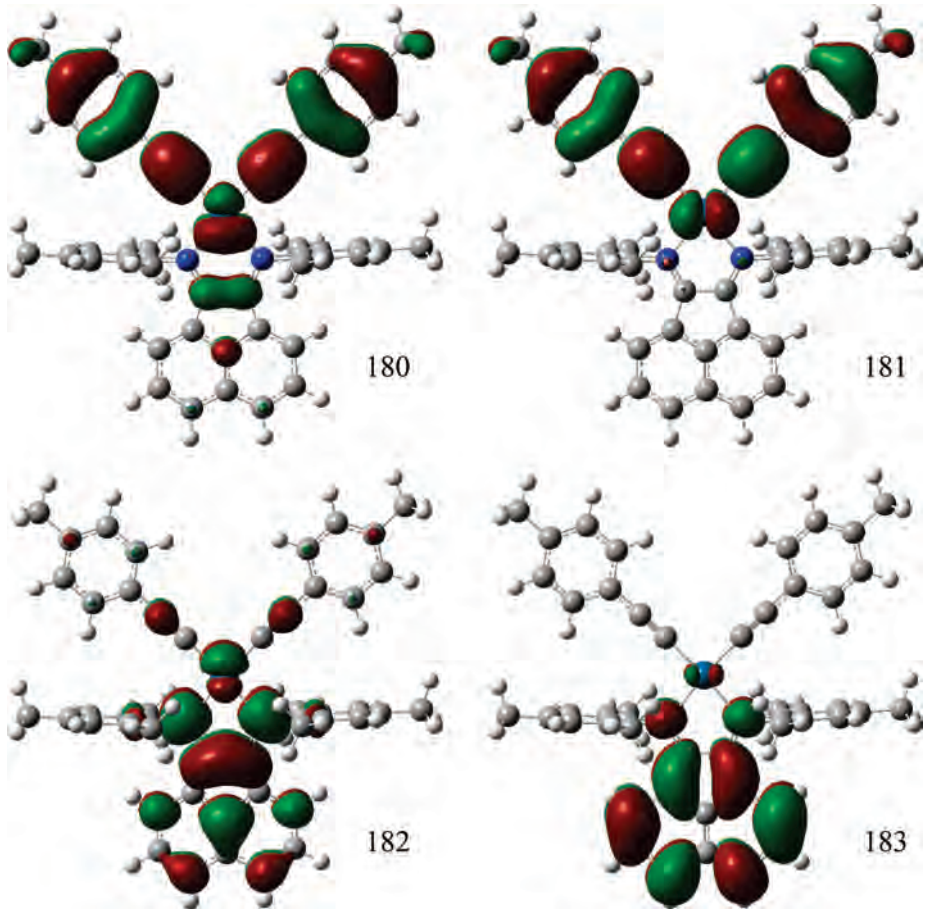

Figure 12. Calculated frontier orbitals of $\mathbf{5s}_{||}$; top to bottom and left to right, orbitals 180, 181 (HOMO), 182 (LUMO) and 183.

calculations show that the only transitions with large oscillator strengths ($f > 0.1$), which would thus be experimentally observable, are those which move electron density between orbitals of the same symmetry. As the recipient orbitals in **5** are predominantly located on the diimine π-system and therefore have a nodal plane containing the platinum atom, the atoms of the diimine system, and the carbon atoms of the triple bonds, then the donor orbitals must fulfill this condition too. When the phenyl rings are coplanar with the diimine ligand this condition is fulfilled by the $\pi_{\perp}$ orbitals, but when the phenyl rings are perpendicular to the plane this condition is fulfilled by the $\pi_{||}$ orbitals. Thus, the orbitals from which the strong low-energy transitions originate differ between the complexes $\mathbf{5s}_{\perp}$ (rings perpendicular) and $\mathbf{5s}_{||}$ (rings parallel); in the former it is the $\pi_{||}$ orbitals and in the latter the $\pi_{\perp}$. Because the $\pi_{||}$ lie lower in energy than the $\pi_{\perp}$, the lowest energy strong transition in $\mathbf{5s}_{\perp}$ is of greater energy than in $\mathbf{5s}_{||}$ because it originates from a lower energy orbital. Details of the low-energy transitions are given in Table 8, and pictures of the pertinent orbitals for $\mathbf{5s}_{||}$ are shown in Figure 12. A more complete set of orbitals for all three geometries is given in the Supporting Information.

The situation is a little more complicated in the model **5sx**, where the two tolyl rings are approximately perpendicular to each other. Essentially the two highest energy transitions are each from one carbon−carbon π-bonding orbital to the LUMO, one from the $\pi_{\perp}$ orbital of the coplanar ring and one from the $\pi_{||}$ orbital of the perpendicular ring.

Table 8. Low-Energy Singlet−Singlet UV-visible Transitions Computed for **5** in Various Geometries[a]

geometry	excited state	orbitals	coefficients	wavelength/nm	oscillator strength
$\mathbf{5s}_{\perp}$	6	178 → 182	0.65	505	0.32
		179 → 183	0.14		
$\mathbf{5s}_{||}$	1	181 → 182	0.69	782	0.06
	2	180 → 182	0.66	622	0.34
		181 → 183	−0.10		
	6	181 → 183	0.69	497	0.09
5sx	2	179 → 182	0.13	728	0.10
		180 → 182	0.67		
	3	178 → 182	−0.11	542	0.24
		179 → 182	0.64		
		180 → 182	−0.11		
		180 → 183	−0.14		
	8	179 → 182	0.12	482	0.10
		180 → 183	0.68		

[a] No more transitions with oscillator strengths greater than 0.02 were computed amongst the ten lowest energy transitions for each geometry.

Importantly, this reveals that breaking the symmetry of the system does not alter the origin of the bands seen in the UV/visible spectrum.

None of our model geometries are a true representation of the molecular conformation in solution simply because they are static, while in reality the aryl rings will readily undergo rotation. Undoubtedly this rotation would allow simultaneous mixing of the metal d-orbitals with both of the π-orbitals on each ligand and thus make the HOMO include a mixture of the two types of π-bonds, parallel and perpendicular. However, the calculations do suggest that

Table 9. Crystal Data and Structure Refinement Details

structure	**4**·2$CHCl_3$	**5**	Pt(MesBIAN)Cl_2·Et_2O
empirical formula	C48 H40 Cl6 N2 Pt1	C48 H42 N2 Pt	C34 H38 Cl2 N2 O1 Pt1
formula weight	1052.6	841.92	756.66
temperature	173(2) K	173(2) K	100(2) K
wavelength	0.71073 Å	0.71073 Å	0.71073 Å
crystal system	triclinic	orthorhombic	orthorhombic
space group	$P\bar{1}$	$P2_12_12_1$	*Pbca*
unit cell dimensions	a = 9.855(9) Å b = 10.455(8) Å c = 23.113(13) Å α = 98.69(7)° β = 98.50(6)°. γ = 102.44(7)°.	a = 11.66180(10) Å b = 14.5179(2) Å c = 22.3442(3) Å α = 90° β = 90° γ = 90°	a = 16.6560(2) Å b = 16.8528(2) Å c = 23.1881(3) Å α = 90° β = 90° γ = 90°
volume	2258(3) $Å^3$	3782.98(8) $Å^3$	6508.90(14) $Å^3$
Z	2	4	8
density (calculated)	1.548 Mg/m^3	1.478 Mg/m^3	1.546 Mg/m^3
absorption coefficient	3.497 mm^{-1}	3.745 mm^{-1}	4.510 mm^{-1}
reflections collected	18561	27335	63943
Independent reflections	10268 [R(int) = 0.0838]	10128 [R(int) = 0.0361]	11472 [R(int) = 0.0550]
Data/restraints/parameters	10268/0/520	10128/0/468	11472/0/369
goodness-of-fit on F^2	1.022	0.916	1.131
final R indices [$I > 2\sigma(I)$]	$R1$ = 0.0794, $wR2$ = 0.1642	$R1$ = 0.0265, $wR2$ = 0.0417	$R1$ = 0.0424, $wR2$ = 0.0837
R indices (all data)	$R1$ = 0.1299, $wR2$ = 0.1875	$R1$ = 0.0399, $wR2$ = 0.0435	$R1$ = 0.0756, $wR2$ = 0.0997
largest diff. peak and hole	5.636 and −2.124 e $Å^{-3}$	2.014 and −1.080 e $Å^{-3}$	3.525 and −2.169 e $Å^{-3}$
absolute structure parameter		−0.012(4)	

whatever the orientation of the rings, the origin of the low-energy transitions seen in the UV/vis is an orbital composed largely of C≡C character with some contribution (between 20 and 40%) from the metal. The transitions are thus mixed metal−ligand to ligand (MMLL′CT) in nature.

Previously, DFT calculations using the same methodology as reported herein have been reported on the related bipyridyl compound [Pt(dbbpy)(−C≡C−C_6H_5)$_2$], in which the emissive state was also assigned as MMLL′CT.[44] In this case, the singlet geometry optimized to a structure with C_2 symmetry, with the phenyl rings at 34° to the plane containing the diimine and the platinum atom, whereas the triplet structure had both rings in the plane, mirroring our results on **5**. The reported energies of the HOMO and LUMO in this calculation were −5.30 and −2.39 eV, respectively, compared to approximately −5.3 and −3.1 eV in our calculations on **5**, thus confirming that the MesBIAN has a lower energy LUMO than the dbbpy but that similar acetylides give HOMOs with similar energies.

Intrigued by the TRIR spectrum of **5**, we undertook some frequency calculations on the triplet state of [Pt(dbbpy)(−C≡C−Ph)$_2$] as the above work[44] did not report these. We found the same excited-state geometry, both phenyl rings lying in the plane of the diimine, and also that the only two frequencies calculated between 1650 and 3000 cm^{-1} were the asymmetric and symmetric combinations of the CC triple bond vibrations, at 1948 and 2138 cm^{-1}, respectively. Similar to our results for **5**, the lower energy vibration is predicted to have a much greater intensity. The reported experimental TRIR study of the similar compound [Pt(dbbpy)(−C≡C−C_6H_4−CH_3)$_2$][8] reports a single band in the excited state at 2150 cm^{-1}, but only reports data down to 2080 cm^{-1}; thus, if the second calculated band is present, it would not have been observed.

Conclusions

The new platinum(II)−acetylide−diimine complexes bearing the strongly electron accepting ligand MesBIAN expand the range of NIR emitters which possess surprisingly long excited-state lifetimes, sufficient to generate singlet oxygen upon irradiation of solutions at room temperature. A combination of absorption and emission spectroscopy, ESR, spectroelectrochemistry, and TD-DFT calculations allowed for an assignment of the nature of the emissive excited state as MMLL′CT, with a considerable contribution from the acetylide moiety. This assignment is further supported by TRIR spectroscopy on the pico- to nanosecond time scales. The TRIR data show a decrease in the energy of ν(C≡C) upon excitation, which is consistent with a charge transfer to a diimine excited state that removes electron density from the carbon−carbon triple bond. The structure of the excited state in **5** is best described as "pseudo-cumulenic", with a high degree of electron density delocalization across the molecule. The structural change upon promotion to the excited state is reflected in an order of magnitude increase of the intensity of the IR signal attributed to ν(C≡C), and in the appearance of an even more intense, extremely broad transient IR band in the range typical for pseudo-cumulenic structures (1820 cm^{-1}).[7] Such "pseudo-cumulenic" structure has never been reported before for platinum(II) diimine chromophores, and opens up potential for applications in electronics and photonics. The picosecond TRIR studies allowed for the determination, for the first time, of the rate of vibrational relaxation of the −C≡C− bond attached to a metal center.

Experimental Details

[Pt(MesBIAN)Cl_2] and [Pt(MesBIAN)(−C≡C−C_6H_4−CF_3)$_2$] **3** were prepared as reported.[10] Alkynes were purchased and used as received. Preparations of new compounds were carried out under nitrogen using dried solvents. NMR spectra were obtained in $CDCl_3$ on a JEOL ECP300 spectrometer and referenced to $SiMe_4$. ESR spectra were recorded on a Bruker ESP300E spectrometer calibrated with dpph, and simulated using Bruker Simfonia. Radicals were generated by freezing a 2:1 THF/CH_2Cl_2 solution of the appropriate neutral compound in an ESR tube in the ESR cavity, adding the

reductant [Co(C_5Me_5)$_2$] to the top, and allowing the solution to warm until a signal was observed. Microanalysis was carried out by the microanalytical laboratory of the University of Bristol School of Chemistry. Electrochemical studies were carried out using an EG&G model 273A potentiostat linked to a computer using EG&G Model 270 Research Electrochemistry software in conjunction with a three-electrode cell. The auxiliary electrode was a platinum wire and the working electrode a platinum disk (1.6 mm diameter). The reference electrode was an aqueous saturated calomel electrode separated from the test solution by a fine porosity frit and an agar bridge saturated with KCl. Solutions in CH_2Cl_2 were 1.0×10^{-3} mol dm^{-3} in the compound and 0.1 mol dm^{-3} in [NBu^n_4][PF_6] as the supporting electrolyte. Under these conditions, $E^{o\prime}$ for the one-electron oxidation of [Fe(η-C_5H_5)$_2$], added to the test solutions as an internal calibrant, is 0.47 V.[58]

Syntheses. [Pt(MesBIAN)(-C≡C−C_6H_5)$_2$] 4. A 0.118 g quantity (0.173 mmol) of [Pt(MesBIAN)Cl_2] and a catalytic amount (<1 mg) of copper(I) iodide were dissolved in 20 mL of CH_2Cl_2 and 1 mL of triethylamine. To this was added 0.076 mL (0.69 mmol) of phenylacetylene, and the mixture stirred for 24 h, during which time it became purple. It was then evaporated to dryness and purified by column chromatography on grade III alumina (25 cm × 4 cm), using CH_2Cl_2 as eluent. The product was collected as a purple band, which was reduced in volume on a rotary evaporator to approximately 25 mL. An approximately equal volume of hexane was then added and evaporation slowly continued until the desired product separated out as dark purple microcrystals. These were isolated by filtration, washed with hexane and dried to give 0.106 g (0.130 mmol, 75%) of product.

[Pt(MesBIAN)(−C≡C−C_6H_4−CN-p)$_2$] **1**, [Pt(MesBIAN)(−C≡C−C_6H_4−CF_3-p)$_2$] **3**, and [Pt(MesBIAN)(−C≡C−$SiMe_3$)$_2$] **2** were prepared similarly from [Pt(MesBIAN)Cl_2] and the appropriate alkyne. So was [Pt(MesBIAN)(−C≡C−C_6H_4−CH_3-p)$_2$] **5**, except that the precipitation from dichloromethane was effected with diethyl ether.

[{Pt(MesBIAN)(−C≡C−$SiMe_3$)$_2$}-η^2,η^2-CuCl] 2a. A 0.054 g quantity (0.079 mmol) of [Pt(MesBIAN)Cl_2], 0.25 mL of trimethylsilylacetylene (1.75 mmol), and 0.023 g of copper(I) chloride (0.23 mmol) were stirred for 16 h in 10 mL of CH_2Cl_2 and 1 mL of triethylamine. The resulting brown solution was then evaporated to dryness and washed three times with saturated sodium chloride solution and once with distilled water. It was then dried over magnesium sulfate, which was removed by filtration prior to the solution being evaporated to dryness again. Trituration of the residue with diethyl ether gave 0.030 g (0.033 mmol) of **2a** as a brown solid.

[Pt(MesBIAN)I_2] 6. To a solution of 0.056 g (0.068 mmol) of **4** in 5 mL of CH_2Cl_2 was added 5 mL of a 17 mM solution of iodine (0.085 mmol). The resulting solution was stirred for 36 h, and then 40 mL of hexane was added. Continued stirring caused the deposition of a dark solid, which was isolated by filtration, washed with hexane, and dried in vacuo to give 0.040 g (0.046 mmol, 68%) of **6**. Treatment of the remaining solution with activated charcoal, filtration and evaporation yielded a light colored solid. This was identified as 1,4-diphenylbuta-1,3-diyne by NMR, IR (ν{C≡C} = 2195s cm^{-1}) and EI-MS (M^+ = 202).

Emission Spectroscopy. Emission experiments were performed at room temperature on CH_2Cl_2 solutions degassed by freeze−pump−thaw methods. Emission spectra were recorded on a home-built system (Sheffield) comprising a Coherent CW Ar ion laser (<10 mW at the sample, 514.5 nm), Bentham TMC600 spectrograph, and Andor iDUS CCD camera. The spectrograph and CCD detection system was calibrated with a Bentham CL2 tungsten calibration lamp. The emission spectra were corrected for the overall system sensitivity.

Luminescence quantum yields were determined relative to [Ru(bpy)$_3$$Cl_2$] in air saturated water, $\phi_o = 0.028$, or relative to a solution of [Pt(MesBIAN)Cl_2] in deoxygenated CH_2Cl_2 ($\phi = 3 \times 10^{-4}$).[10] Luminescence lifetimes were measured with a Mini-τ fluorimeter (Edinburgh Instruments) containing a picosecond diode laser (410 nm, 80 ps) as an excitation source; the emission wavelength range was selected by glass filters. Experimental uncertainties are estimated to be 20% for emission quantum yields and 15% for luminescence lifetimes.

The nanosecond and picosecond TRIR experiments were performed at the Central Laser Facility of the Rutherford Appleton Laboratory (RAL), STFC, U.K. The experiments were carried out in tetrahydrofuran (THF) or CH_2Cl_2 solutions under an inert atmosphere, with a standard concentration of approximately 1 mM; concentration dependence studies were done in the range between 1 mM and 46 μM.

The picosecond-TRIR setup at RAL has been described in detail elsewhere.[43] Briefly, part of the output from a 1 kHz, 800 nm, 150 fs, 1 mJ Ti:Sapphire oscillator/regenerative amplifier was used to pump a white light continuum seeded BBO OPA. The signal and idler produced by this OPA were difference frequency mixed in a type I $AgGaS_2$ crystal to generate tuneable mid-infrared pulses (ca. 150 cm^{-1} fwhm, 0.1 μJ). Second harmonic generation of the residual 800 nm light provided 400 nm pulses, which were used to excite the sample (typical excitation energy 3 μJ, focus 100 μm^2). Changes in infrared absorption were recorded by normalizing the outputs from a pair of 64-element HgCdTe linear array detectors on a shot-by-shot basis. The nanosecond TRIR setup, described in detail elsewhere,[59] combines the PIRATE TRIR spectrometer and nanosecond AOT-YVO-20QSP/MOPA Nd:Vanadate diode pumped microlaser, with a pulse duration of 0.6 ns and energies of about 0.6 μJ/pulse.

Computational Studies. All calculations were performed with Gaussian 03 (Revision C.02)[60] and used the popular B3LYP density functional.[61−63] The Stuttgart−Dresden (SDD) basis set[64] was used with a relativistic effective core potential for Pt, and all ligand atoms (C, H, N) were described by the all-electron 6−31G* basis set. In agreement with results reported by other groups, we found that

(58) Connelly, N. G.; Geiger, W. E. *Chem. Rev.* **1996**, *96*, 877–910.

(59) Towrie, M.; Gabrielsson, A.; Matousek, P.; Parker, A. W.; Rodriguez, A.-M. B., Jr. *Appl. Spectrosc.* **2005**, *59*, 467.

(60) Frisch, M. J.; Trucks, G. W.; Schlegel, H. B.; Scuseria, G. E.; Robb, M. A.; Cheeseman, J. R.; Jr., J. A. M.; Vreven, T.; Kudin, K. N.; Burant, J. C.; Millam, J. M.; Iyengar, S. S.; Tomasi, J.; Barone, V.; Mennucci, B.; Cossi, M.; Scalmani, G.; Rega, N.; Petersson, G. A.; Nakatsuji, H.; Hada, M.; Ehara, M.; Toyota, K.; Fukuda, R.; Hasegawa, J.; Ishida, M.; Nakajima, T.; Honda, Y.; Kitao, O.; Nakai, H.; Klene, M.; Li, X.; Knox, J. E.; Hratchian, H. P.; Cross, J. B.; Adamo, C.; Jaramillo, J.; Gomperts, R.; Stratmann, R. E.; Yazyev, O.; Austin, A. J.; Cammi, R.; Pomelli, C.; Ochterski, J. W.; Ayala, P. Y.; Morokuma, K.; Voth, G. A.; Salvador, P.; Dannenberg, J. J.; Zakrzewski, V. G.; Dapprich, S.; Daniels, A. D.; Strain, M. C.; Farkas, O.; Malick, D. K.; Rabuck, A. D.; Raghavachari, K.; Foresman, J. B.; Ortiz, J. V.; Cui, Q.; Baboul, A. G.; Clifford, S.; Cioslowski, J.; Stefanov, B. B.; Liu, G.; Liashenko, A.; Piskorz, P.; Komaromi, I.; Martin, R. L.; Fox, D. J.; Keith, T.; Al-Laham, M. A.; Peng, C. Y.; Nanayakkara, A.; Challacombe, M.; Gill, P. M. W.; Johnson, B.; Chen, W.; Wong, M. W.; Gonzalez, C.; Pople, J. A.; *Gaussian 03*, Rev. C.02; Gaussian, Inc.: Pittsburgh PA, 2003.

(61) Lee, C. T.; Yang, W. T.; Parr, R. G. *Phys. Rev. B* **1988**, *37*, 785–789.

(62) Becke, A. D. *J. Chem. Phys.* **1993**, *98*, 5648–5652.

(63) Vosko, S. H.; Wilk, L.; Nusair, M. *Can. J. Phys.* **1980**, *58*, 1200–1211.

(64) Andrae, D.; Haeussermann, U.; Dolg, M.; Stoll, H.; Preuss, H. *Theor. Chim. Acta* **1990**, *77*, 123.

changing the basis set or the density functional had little effect on the calculated transitions and orbital compositions.[65,66] All calculations were performed in a dichloromethane ($\varepsilon = 8.93$) continuum solvation field, using the default polarizable continuum model PCM[67,68] as implemented in G03 with radii from the UFF force field (explicit hydrogens). To avoid problems with cavity generation and slow convergence, solvated calculations were run without symmetry, and some scrf solvation parameters were changed from their default settings (ofac = 0.8, rmin = 0.5). Orbital symmetry labels were confirmed by optimization and TD-DFT in vacuo with C_{2v} symmetry; despite optimizations without symmetry, we observed no significant departure from these geometries. Typically, TD-DFT calculations[69−71] were used to calculate the 10−15 lowest singlet transitions. Because of the size of the complex (93 atoms, no symmetry), loose geometry optimization criteria were used. Molecular orbital compositions were calculated as described by Liu et al.[72] Frequency calculations were performed in the gas-phase without solvation and with symmetry constrained (apart from **5sx**) gas-phase geometries.

Crystal Structure Determination. Summary X-ray crystallographic data is presented in Table 9. Diffraction intensities were collected on a Bruker SMART APEX CCD diffractometer, with graphite-monochromated Mo Kα (0.71073 Å) radiation. The data were corrected for absorption. The structures were solved by SHELXS-97, expanded by Fourier-difference syntheses, and refined with the SHELXL-97 package incorporated into the SHELXTL crystallographic package. The position of the hydrogen atoms were calculated by assuming ideal geometries but not refined. All non-hydrogen atoms were refined with anisotropic thermal parameters by full-matrix least-squares procedures on F^2.

Acknowledgment. We thank Johnson-Matthey for a generous loan of platinum metal salts. J.A.W. is grateful to the EPSRC (GR/T03345) and to the Royal Society for support and to the Rutherford Appleton Laboratory, Science and Technology Funding Council, for TRIR beam time. N.F. and C.J.A. wish to thank the University of Bristol for employment. N.F. thanks the EPSRC for the award of an Advanced Research Fellowship (EP/E059376/1). I.V.S. thanks the E.U. for a Marie Curie Incoming International Fellowship (MIF1-CT-2006-040168).

Supporting Information Available: Thermal ellipsoid plots of **5** and [Pt(MesBIAN)Cl_2]·Et_2O are available as electronic Supporting Information, and the full structural and refinement details are available as cif files. Pictures of the frontier orbitals for the model geometries **5sx**, $\mathbf{5s}_{\perp}$, and $\mathbf{5s}_{\parallel}$ are also included, as are diagrams showing the nanosecond TRIR spectra of **5** in dichloromethane and **4** in THF. This material is available free of charge via the Internet at http://pubs.acs.org.

IC800850H

(65) Hay, P. J. *J. Phys. Chem. A* **2002**, *106*, 1634–1641.
(66) Petit, L.; Maldivi, P.; Adamo, C. *J. Chem. Theory Comput.* **2005**, *1*, 953–962.
(67) Cossi, M.; Barone, V. *J. Chem.Phys.* **2001**, *115*, 4708–4717.
(68) Cossi, M.; Scalmani, G.; Rega, N.; Barone, V. *J. Chem.Phys.* **2002**, *117*, 43–54.
(69) Bauernschmitt, R.; Ahlrichs, R. *Chem. Phys. Lett.* **1996**, *256*, 454.
(70) Casida, M. E.; Jamorski, C.; Casida, K. C.; Salahum, D. R. *J. Chem.Phys.* **1998**, *108*, 4439.
(71) Stratmann, R. E.; Scuseria, G. E.; Frisch, M. J. *J. Chem.Phys.* **1998**, *109*, 8218–8224.
(72) Liu, X.-J.; Feng, J.-K.; Meng, J.; Pan, Q.-J.; Ren, A.-M.; Zhou, X.; Zhang, H.-X. *Eur. J. Inorg. Chem.* **2005**, *185*, 6–1866.